Along-strike variations in the fossil subduction zone of the Western Alps revealed by the CIFALPS seismic experiments and their implications for exhumation of (ultra-) high-pressure rocks

Anne Paul, Marco G Malusà, Stefano Solarino, Simone Salimbeni, Elena Eva, Ahmed Nouibat, Silvia Pondrelli, Coralie Aubert, Thierry Dumont, Stephane Guillot, et al.

Accepted for publication in Earth and Planetary Science Letters, Oct. 25, 2022 (Ms. # EPSL-D-22-00914)

Along-strike variations in the fossil subduction zone of the Western Alps revealed by the CIFALPS seismic experiments and their implications for exhumation of (ultra-) high-pressure rocks

Anne Paul [1*], Marco G. Malusà [2*], Stefano Solarino [3], Simone Salimbeni [4], Elena Eva [3], Ahmed Nouibat [1], Silvia Pondrelli [4], Coralie Aubert [1], Thierry Dumont [1], Stéphane Guillot [1], Stéphane Schwartz [1], Liang Zhao[5*]

[1] Univ. Grenoble Alpes, Univ. Savoie Mont Blanc, CNRS, IRD, UGE, ISTerre, Grenoble, France

[2] Department of Earth and Environmental Sciences, University of Milano-Bicocca, Piazza della Scienza 4, 20126 Milan, Italy

[3] Istituto Nazionale di Geofisica e Vulcanologia, ONT, Genova, Italy

[4] Istituto Nazionale di Geofisica e Vulcanologia, Bologna, Italy

[5] State Key Laboratory of Lithospheric Evolution, Institute of Geology and Geophysics, Chinese Academy of Sciences, Beijing, China

*Corresponding authors: anne.paul@univ-grenoble-alpes.fr, marco.malusa@unimib.it, zhaoliang@mail.iggcas.ac.cn

Abstract

In complex plate-boundary settings, a reliable 3-D geophysical characterization of the deep tectonic structure is a fundamental starting point for a breakthrough in the analysis of processes controlling plate subduction and (U)HP rock exhumation. The Western Alps host one of the best-studied fossil subduction zones worldwide, with a well-defined deep structure in 2-D based on recent geophysical experiments. However, a full 3-D characterization of its deep tectonic structure is still lacking. Here we present a series of new receiver function cross-sections across the northern and southern Western Alps, validated and complemented by a S-wave velocity model from ambient-noise tomography that provides additional constraints between the profiles. We document a marked change in Moho attitude from the northern Western Alps, where the eastward-dipping European Moho reaches ~45 km depth beneath the Gran Paradiso

dome, to the southern Western Alps, where the European Moho reaches ~70 km depth beneath the equivalent Dora-Maira dome. This change in Moho attitude takes place over a few tens of kilometers and was likely emphasized by deformation of the slab during subduction. The Western Alps subduction wedge is much thicker in the south than in the north, and the mantle-wedge rocks are deeply involved in orogeny exclusively in the south, where coesite is found in continental (U)HP rocks at several locations. Our detailed information on the 3-D structure of the subduction wedge provides first-order constraints for the next-generation of thermo-mechanical numerical models and may help explain the lateral variations in exhumation style revealed by the geologic record.

Keywords: seismic tomography, continental subduction, exhumation, Western Alps

Highlights:

- New receiver function sections from a recent seismic experiment across the NW Alps
- 2D receiver functions profiles complemented by a 3D Vs model from ambient noise
- Strong change in Moho attitude between NW and SW Alps
- The Western Alps subduction wedge is much thicker in the south than in the north
- A steeper Moho beneath locations where coesite is found in continental UHP rocks

1. Introduction

The Western Alps are one of the best-preserved fossil subduction zones worldwide and they have provided the first petrologic evidence of continental subduction with the discovery of coesite in metamorphic rocks of the Dora-Maira massif (Chopin, 1984). Since that discovery, petrologic evidence of continental subduction has been reported from numerous orogenic belts, highlighting the role played by continental subduction in the dynamics of mountain building (e.g., Guillot et al., 2009a and references therein). In the light of these specificities, the Western Alps have long provided key inputs and control for the development of 2-D thermo-mechanical models to investigate continental subduction and exhumation (e.g., Yamato et al., 2008; Butler et al., 2013; Liao et al., 2018). However, the distribution of exposures of continental (ultra-) high-pressure [(U)HP] rocks in the Western Alps and in other orogenic belts shows major lateral changes (Guillot et al., 2009a). Moreover, theoretical models of (U)HP rock exhumation in complex plate-boundary settings (e.g., Webb et al., 2008; Malusà et al., 2011) highlight the importance of a well constrained 3-D tectonic framework for a proper understanding of processes controlling subduction and exhumation. In those situations, a pre-requisite for any reliable 3-D thermo-mechanical modelling is a reliable 3-D geophysical characterization of the deep tectonic structure of the fossil subduction zone and associated subduction wedge, and of

the potential variations in lithospheric structure along strike. This characterization can be particularly informative in those cases where syn-exhumation geometries are demonstrably preserved.

The fossil subduction zone of the Western Alps is extremely well studied, and its deep tectonic structure is well-constrained across the Dora-Maira massif (southern Western Alps) thanks to the CIFALPS passive seismic experiment (Malusà et al., 2021) (Fig. 1). By contrast, the earlier ECORS-CROP normal-incidence seismic reflection experiment (Nicolas et al., 1990) probing the crustal structure of the northern Western Alps (dotted red line in Fig. 1) failed to detect the European Moho beneath the Alpine subduction wedge. Although recent seismic tomography studies have suggested potential along-strike variations in the Alpine seismic structure (e.g., Solarino et al., 2018; Zhao et al., 2020), a complete characterization of the deep structure of the northern Western Alps is still lacking. To tackle this issue, we conceived a new seismic experiment across the northern Western Alps, namely the CIFALPS2 experiment (Zhao et al., 2018) to complement the ECORS-CROP controlled-source seismic profile with high-quality passive seismic data.

In this article, we present a series of new receiver function cross-sections across the northern Western Alps based on new data from the CIFALPS2 experiment, besides an improved receiver function cross-section across the southern Western Alps based on fully reprocessed CIFALPS data. Our receiver function analysis is validated and complemented by a recent ambient-noise tomography study by Nouibat et al. (2022) that provides 3-D constraints on the deep crustal structure in-between the profiles. The resulting seismic images integrate the high-resolution, but substantially 2-D picture provided by the CIFALPS experiment (Malusà et al., 2021), and reveal striking and rapid north-south variations in the seismic structure of the fossil subduction zone of the Western Alps. Our findings are of primary importance to set up conceptual and quantitative modelling of continental subduction, and to understand first-order lateral variations in the styles and mechanisms of (U)HP rock exhumation suggested by the geologic record.

2. Tectonic setting

The Western Alps are the result of oblique subduction of the Alpine Tethys under the Adriatic microplate since the Late Cretaceous, followed by diachronous continent-continent collision between the Adriatic and European paleomargins during the Cenozoic (e.g., Dal Piaz, 2001; Handy et al., 2010; Dumont et al., 2022). European basement rocks and associated cover sequences that escaped Alpine metamorphism are exposed in the External zone of the orogen

to the west of the Frontal Pennine Fault. The European basement preserves relics of a complex Variscan evolution (e.g., Guillot et al., 2009b). It is found not only in the External Massifs (e.g., Mont Blanc and Pelvoux, MB and Pe in Fig. 1), but also farther west beneath the European foreland, where the Bresse Graben records major late Eocene-Oligocene tectonic subsidence (Ziegler, 1992; Sissingh, 2001). The Alpine subduction wedge that was accreted atop the European slab is preserved in the Internal zone of the Western Alps, to the east of the Frontal Pennine Fault (FPF in Fig. 1). It chiefly includes Penninic rocks derived from the Alpine Tethys and from the distal European paleomargin (e.g., Handy et al., 2010). On the upper-plate side of the orogen, eclogitized mantle rocks of the Lanzo massif and Austroalpine-Southalpine rocks, derived from the Adriatic paleomargin, are exposed north of the Po Plain, where the Ivrea gravity anomaly (dashed purple line in Fig. 1) (Bigi et al., 1990; Zahorec et al., 2021) suggests the presence of mantle rocks at upper-crustal depths (Nicolas et al., 1990). South of the Po Plain, the complex transition zone between the Western Alps and the Apennines is partly masked by thick Cenozoic sedimentary successions (Cassano et al., 1986).

Two main tectono-metamorphic domains can be recognized in the Alpine subduction wedge (Fig. 1): (i) an Eocene eclogite belt on the upper-plate side, and (ii) a doubly-vergent frontal wedge consisting of lower-pressure metamorphic rocks on the lower-plate side. Different tectonostratigraphic sections exposed along different transects of the frontal wedge likely reflect the obliquity of the Alpine trench relative to the European paleomargin (Malusà et al., 2015; Dumont et al., 2022).

The Eocene eclogite belt consists of (U)HP continental crust domes of European origin (Dora-Maira, Gran Paradiso and Monte Rosa) tectonically enveloped by (U)HP metaophiolites. These (U)HP rocks reached the pressure peak in the late Eocene and were rapidly exhumed to Earth's surface by the early Oligocene, to be unconformably covered by syntectonic sediments still preserved in the Tertiary Piedmont Basin (e.g., Malusà et al., 2011). The domal shape of the Dora-Maira and Gran Paradiso massifs (DM and GP in Fig. 1) indicates only minor late-stage indentation of the Adriatic upper plate beneath the southern segments of the Alpine subduction wedge after (U)HP rock exhumation. This observation suggests that the geometries related to the (U)HP exhumation stage have not changed since the Oligocene, when Adria-Europe convergence was minor and mainly accommodated in the External Zone of the orogen, as also confirmed by thermochronology data (Malusà et al., 2015). Farther south, the inferred preservation of syn-exhumation geometries is supported by the occurrence of nearly undeformed Oligocene-Miocene sedimentary strata atop the Eocene eclogite belt (e.g., Cassano et al., 1986) (Fig. 1). By contrast, north of the study area, the Monte Rosa dome (MR in Fig. 1)

was evidently backfolded during the latest stages of hard continent-continent collision (Pfiffner et al., 2002), which implies that the geometries related to (U)HP rock exhumation have been strongly modified. These observations are consistent with a much greater amount of collisional shortening in the Central Alps compared to the Western Alps due to the northward motion of Adria relative to Europe.

The first seismic evidence for continental subduction in the Western Alps was provided by the CIFALPS passive experiment with teleseismic phases converted on the European Moho at 75-80 km depth beneath the Dora-Maira (Zhao et al., 2015). These large Moho depth values were later confirmed by full-waveform inversion of teleseismic data and transdimensional ambient-noise tomography using the CIFALPS dataset (Beller et al., 2018; Zhao et al., 2020). According to the joint interpretations of geological and geophysical data along the CIFALPS profile, the thick subduction wedge of the southern Western Alps would consist of a mixture of (U)HP metamorphic rocks of European origin exposed in the Dora-Maira dome as well as subduction channel serpentinite and mantle-wedge peridotite with varying degrees of serpentinization (Malusà et al., 2021). The crustal structure of the northern Western Alps has been probed by the ECORS-CROP controlled-source seismic experiments, including normal-incidence and wide-angle profiles that highlighted the intricate geometries of the European and Adriatic Mohos (Nicolas et al., 1990; ECORS-CROP DSS Group, 1989). The normal-incidence reflection profile failed to detect the European Moho beneath the Internal zone, which was only visible on wide-angle profiles at a maximum depth of 55 km. As a result, the deep structure of the Northwestern internal Alps was poorly constrained prior to the CIFALPS2 experiment.

Coesite is found at several locations within the exhumed continental (U)HP rocks of the Dora-Maira massif (Chopin, 1984; Manzotti et al., 2022), suggesting maximum pressures even greater than ~3.5 GPa. However, it is not found in the Gran Paradiso and Monte Rosa massifs, where the estimated maximum pressures do not exceed ~2.4 GPa (Malusà et al. 2011; Manzotti et al., 2022). This observation suggests potentially relevant lateral variations in exhumation style within the subduction wedge of the Western Alps, which can still be reflected today by the deep tectonic structure of the orogen.

3. Data and Methods

The CIFALPS2 experiment (network code XT; Zhao et al., 2018) includes 55 broadband stations operating for 14 months in 2018–2019, that were roughly aligned along two segments: (i) a WNW-ESE segment from the eastern Massif Central (France) to the region of Ivrea (Italy) across the Bresse Graben, the Jura fold-and-thrust belt, and the northern Western Alps; and (ii)

a NNW-SSE segment from the region of Ivrea to the Ligurian coast across the western Po Plain (Fig. 1). In this paper, we focus on the WNW-ESE segment of the transect, hereafter referred to as the CIFALPS2 main profile. The main profile is ~330 km long and, with additions from the permanent networks (CH, Swiss Seismological Service (SED) At ETH Zurich, 1983; GU, University of Genoa, 1967; IV, INGV Seismological Data Centre, 2006; FR, RESIF, 1995) and AlpArray temporary network (Z3, AlpArray Seismic Network, 2015), includes 43 stations with a dense interstation spacing of 8 km on average. The CIFALPS2 experiment also includes two shorter complementary profiles across the Internal zone of the Western Alps, located to the north (ALP-N, 10 stations) and to the south (ALP-S, 9 stations) of the main profile (Fig. 1). Additional information on technical aspects of the seismic experiment and data quality is provided in Supplementary text S1 and Figure S1.

To image the crustal structure and the Moho beneath the CIFALPS2 main profile and the ALP-N and ALP-S complementary profiles, we used the receiver function analysis that enhances P-to-S converted phases at seismic discontinuities in three-component records of teleseismic earthquakes (Vinnik, 1977; Langston, 1979). We took advantage of the dense array of sensors to extract the scattered wavefield for each event, therefore enhancing the quality of receiver functions by applying the multichannel preprocessing approach (Rondenay, 2009; Millet et al., 2019; see Supplementary text S2 for more details). In regions with complex 3-D structure, this approach is more efficient than the conventional deconvolution of the vertical-component record from the radial-component record (e.g., Zhao et al., 2015). With respect to the conventional Z-R-T processing scheme, it also has the advantage to remove or strongly attenuate the direct P wave at 0s lag time in the receiver functions, therefore enhancing the converted phases from shallow interfaces.

After this deconvolution step, we migrated the radial receiver functions to depth using, for each station, the 1-D shear-wave velocity model extracted from the 3-D ambient-noise tomography model of Nouibat et al. (2022) and a constant Vp/Vs ratio for the crustal part, and the IASP91 Earth model for the mantle part (Kennett and Engdahl, 1991). Finally, we applied the classical common conversion point (CCP) stacking method (Dueker and Sheehan, 1997) to compute depth sections of stacked P-to-S converted phases beneath the main profile of 43 stations. Due to the complex 3-D structure of the Alpine crust, receiver function waveforms are highly variable with the back-azimuth of the incident *P* wave. Seismic anisotropy in the crust can also lead to azimuthal variations of receiver function waveforms. However, based on previous studies on crustal anisotropy estimated from azimuthal variations of receiver functions along the CIFALPS profile (Salimbeni et al., 2021), and on radial anisotropy in the European

crust from ambient noise tomography (Alder et al., 2021), we believe that the complex 3-D structure of the crust, with layer boundaries dipping in various directions, plays a much stronger part than anisotropy in the variations of waveforms with azimuth. Moreover, crustal anisotropy detected by Salimbeni et al. (2021) is mainly located within the Adriatic upper plate, which implies a negligible impact of anisotropy on the analysis of the European Moho and the overlying subduction wedge. With these issues in mind, we selected signals in the back-azimuth range 0-100° to improve the CCP stack and enhance converted phases on east-dipping structures. This selection provides a large number of coherent receiver functions (see earthquake map in Supplementary Fig. S2a). The robustness of the CCP stacks was attested by jackknife tests, the results of which are presented in Supplementary text and Fig. S3.

For the southern Western Alps, we re-processed the records of the CIFALPS experiment (Zhao et al., 2016a) using the same scheme, back-azimuth selection, and crustal *S*-wave velocity model for migration (Nouibat et al., 2022) that we have adopted for the northern Western Alps (Fig. 1). The CCP stacks of the CIFALPS and CIFALPS2 experiments were validated by comparison with a recent ambient-noise tomography study by Nouibat et al. (2022), a totally independent method that we use to test the reliability of the structural images delineated by receiver function analysis (see details in Figs. 2-4 and Sect. 4). We consider this comparison between independent methods as a much better proof of reliability of the CCP stacks than any other type of test.

Finally, our receiver function images were interpreted jointly with the *P*-wave velocity depth sections by Solarino et al. (2018), with data provided by controlled-source seismology (e.g., Cassano et al., 1986; Sénéchal and Thouvenot, 1991), and with the *S*-wave velocity depth sections by Nouibat et al. (2022), which also provide additional constraints on the deep structure in-between the profiles.

4. Results

4.1 CIFALPS2 main profile

Figure 2 shows, for the CIFALPS2 main profile and from top to bottom, the Bouguer anomaly from the new pan-Alpine gravity data base of Zahorec et al. (2021), the geological map around the main profile, the interpretive geologic cross-section resulting from the joint interpretation of geological and geophysical constraints (see next section), the CCP stack, the *S*-wave velocity section through the model of Nouibat et al. (2022) and the *P*-wave velocity section through the model of Solarino et al. (2018). Since the ECORS-CROP normal-incidence

deep seismic reflection profile (dashed red line in Fig. 1) was located close to the CIFALPS2 Alpine section, the interpretation also uses the depth migrated line drawing of ECORS-CROP (Sénéchal and Thouvenot, 1991) superimposed on the CCP stack, as shown in Supplementary Fig. S3.

On the lower-plate side of the CIFALPS2 main profile, the CCP stack displays laterally continuous *P*-to-*S* (*Ps*) converted phases of positive polarity and strong amplitude, labelled "1" in Fig. 2d. They correspond to the European Moho dipping gently from ~25 km depth at the north-western end of the profile to ~45 km depth at distance 260 km beneath the Gran Paradiso dome (GP in Fig. 2b) and the western tip of the Adriatic upper plate. To delineate the European Moho more precisely, we picked the 4.3 km s^{-1} *S*-wave velocity contour of Fig. 2e. This contour matches well the *Ps* phases of Fig. 2d even at depths between 55-65 km and distances between 260-300 km, where the quality of the CCP stack is poorer due to the higher seismic noise in the Po Plain and strong amplitude near-surface multiples (labelled M in Fig. 2d). Beneath the Mont Blanc Massif (MB in Fig. 2b), the Vs model of Nouibat et al. (2022) displays the same Moho step as the ambient-noise tomography of Lu et al. (2018).

On the upper-plate side of the profile, the Adriatic Moho is more poorly detected by the receiver functions compared to the European Moho, due to the low signal-to-noise ratio and ringing waves in the poorly consolidated sediments of the Po Plain (label "2" in Fig. 2d). It is however clearly imaged by the high-frequency waves of the ECORS-CROP controlled-source seismic section, in close correspondence with the 4.3 km s^{-1} Vs contour (Supplementary Fig. S3). In the Adriatic crust, the *S*-wave velocity contour bounding the bedrock of the Po basin shows a vertical offset (Fig. 2d) consistent with backthrusting of the whole Adriatic crust as proposed by previous interpretations of the ECORS-CROP profile (e.g., Roure et al., 1990).

As in the CIFALPS profile (Zhao et al., 2015), the CCP stack shows a set of diffuse negative-polarity *Ps* converted phases in-between the shallow Adriatic Moho and the deep European Moho beneath the subduction wedge and the tip of the upper plate (label "3" in Fig. 2d). These negative-polarity signals outline a steeply southeast-dipping interface that intersects the surface at the Frontal Pennine Fault (FPF in Fig. 2b), which is the structural boundary separating the metamorphic units of the Alpine subduction wedge in the east from the unmetamorphosed rocks of the European lower plate in the west. The Vs model shows that this dipping boundary corresponds, in the 20-40 km depth range, to a 10-15 km thick zone of diffuse velocity decrease with depth, between the rather high seismic velocities of the subduction wedge and overlying serpentinized mantle wedge above (~3.7-3.8 km s^{-1}), and the weaker velocities of the European crust below (~3.5 km s^{-1}).

In the European crust, we recognized four sets of *Ps* converted phases labelled "4" to "7" in Fig. 2d. These interfaces closely correspond to velocity changes in the *S*-wave velocity section of Fig. 2e. The shallow positive-polarity conversion labelled "4" coincides with the strong velocity increase at the base of the Mesozoic cover of the Jura and Subalpine chains. The sharp positive and negative polarity converted phases labelled "5" and "6" bound a high-velocity body (Vs ~3.7 km s^{-1}) in the mid-crust (7-15 km depth) beneath the Bresse Graben, also extending beneath the western Jura fold-and-thrust belt to the east and the Massif Central to the west. The laterally discontinuous negative-polarity conversion labelled "7" is near-parallel to the European Moho and marks the top of two low-Vs anomalies (minimum 3.3 km s^{-1}) located in the European lower crust on both sides of the previously mentioned Moho step. The lateral change in polarity of converted phases in Fig. 2d coincides with the zone of slightly higher Vs that separates the two anomalies right above the Moho step.

4.2 ALP-N and ALP-S complementary profiles

Figure 3 shows the Bouguer anomaly, CCP stack and S-wave velocity section (Nouibat et al., 2022) for the ALP-N and ALP-S complementary profiles across the subduction wedge of the northern Western Alps. On the ALP-N profile, the CCP stack displays laterally continuous *Ps* converted phases of positive polarity and strong amplitude corresponding to the European Moho ("1" in Fig. 3c). They dip gently from ~35 km depth beneath the Mont Blanc massif (MB in Fig. 3b) to ~60 km depth beneath the Sesia-Lanzo unit (Se in Fig. 3b). This interface matches well the 4.3 km s^{-1} velocity contour in the *S*-wave velocity section of Fig. 3d, especially from 0 to 90 km along the horizontal axis. Positive-polarity *Ps* converted phases corresponding to the Adriatic Moho, labelled "2" in Fig. 3c, are detected on the upper-plate side of the profile. A set of diffuse negative-polarity *Ps* converted phases, labelled "3" in Fig. 3c, is observed above the European Moho beneath the subduction wedge. As in Fig. 2b, this shallow-dipping interface intersects the surface at the Frontal Pennine Fault. The Vs model shows that this boundary, in the 15-35 km depth range, corresponds to a 10-km-thick zone of diffuse velocity decrease with depth (Fig. 3d).

On the ALP-S profile, the positive-polarity *Ps* converted phases marking the European Moho define a steeply dipping interface ("1" in Fig. 3g) from ~45 km depth beneath the Gran Paradiso dome to ~75 km depth beneath the Ivrea-Verbano zone (IV in Fig. 3f). At depths > 50 km, this interface is better constrained by the 4.3 km s^{-1} Vs contour (Fig. 3h) rather than by the low-amplitude *Ps* conversions of the CCP section (Fig. 3g). The set of diffuse negative-polarity converted *Ps* phases detected above the European Moho (label "3" in Fig. 3) is much steeper

than in Fig. 3d, and near-parallel to the European Moho along the ALPS-S profile. In the 20-60 km depth range, these negative-polarity converted phases correspond to a 10-km-thick zone of diffuse velocity decrease with depth in the Vs section (Fig. 3h).

4.3 Re-processed CIFALPS profile

Figure 4 shows the same information as Fig. 2 for the re-processed CIFALPS transect located farther south in the southern Western Alps. The improved CCP section of Fig. 4d enhances the converted phases from shallow interfaces and, when compared to the original analysis by Zhao et al. (2015), provides further information on the lithospheric structure of both the Adriatic and European plates, whereas no major improvement is introduced for the subduction wedge (Malusà et al., 2021). This information is consistent with indications provided by the Vs model of Fig. 4e and by controlled-source seismic data in the Po Plain (e.g., Cassano et al., 1986).

As shown in Fig. 4d-e, the European Moho along the CIFALPS profile (label *"1"*) is better constrained at depth > 45 km by the 4.3 km s^{-1} Vs contour (Fig. 4e) rather than by the low-amplitude *Ps* conversions of the CCP section (Fig. 4d), like what is observed in the ALP-S complementary profile. The Moho dip angle is steeper than in the CIFALPS2 section (Fig. 2d-e) and, at depths > 60 km, is likely steeper than suggested by the previous CIFALPS studies (e.g., Zhao et al., 2015; Beller et al., 2018). The low amplitudes of the *Ps* conversions are coherent with the weak velocity gradient shown by the Vs section between the subducted, possibly eclogitized European lower crust and the underlying lithospheric mantle. The *Ps* conversions marking the Adriatic Moho (label "2" in Fig. 4d-e) are offset by faults already described in previous work (Zhao et al., 2015; Malusà et al., 2017; Solarino et al., 2018) and fully consistent with undulations of the *S*-wave velocity contours (Fig. 4e). Integration with information provided by the Vs model allows us to trace these faults at even greater depths in the Adriatic mantle lithosphere compared to previous studies.

The set of negative-polarity *Ps* phases labelled "3" in Fig. 4d is more diffuse with weaker amplitudes than in Fig. 2d, probably due to the presence of a thicker subduction channel along the CIFALPS profile (Zhao et al., 2020) and a weak velocity contrast with the partly serpentinized Adriatic mantle on its top (Fig. 4e). Above this set of negative-polarity phases, the *P*-wave velocity contour 6.7 km s^{-1} in Fig. 4f was interpreted by Solarino et al. (2018) as marking the upper and western boundary of a serpentinized mantle body located underneath the (U)HP rocks of the Dora-Maira dome (DM in Fig. 4c). This velocity boundary crosscuts the Vs contours of Fig. 4e at a high angle, leaving out the western tip of a high-Vs body (Vs=3.8-

4.15 km s^{-1}) at 15-30 km depth (marked by a star in Fig. 4e-f) that shows rather low, more crust-like *P*-wave velocities (Vp=5.9-6.4 km s^{-1}).

In the Adriatic crust, the base of the Oligocene-to-Quaternary sediments of the Tertiary Piedmont Basin and western Po Plain can be delineated as a set of positive-polarity *Ps* conversions (label "4" in Fig. 4d) that correspond to the Vs structure in Fig. 4e. Farther east, the Monferrato frontal thrust is marked by a set of south-dipping negative-polarity Ps conversions (label "5" in Fig. 4d) consistent with evidence from available seismic-reflection profiles (e.g., Cassano et al., 1986). These negative-polarity *Ps* conversions show a step along the Villalvernia-Varzi Fault (VVF in Fig. 4), consistent with the Neogene activity of the fault.

In the western side of the CIFALPS profile, the European crust includes, similar to CIFALPS2, a strong low-Vs anomaly (minimum 3.2 km s^{-1}) located beneath the Subalpine Chains, bounded on top by a set of sharp negative-polarity *Ps* conversions labelled "6" in Figs. 4d-e. The crust beneath the Rhône Valley shows rather high *S*-wave velocities, similar to the Bresse Graben in the CIFALPS2 section.

5. Interpretation and discussion

5.1 CIFALPS2 vs CIFALPS geologic cross-sections

The new crustal-scale geological cross-section of the northern Western Alps along the CIFALPS2 main profile has some similarities with the previously proposed cross-section of the southern Western Alps (CIFALPS experiment, see Malusà et al., 2021), but also some major differences (cf. Fig. 2c and Fig. 4c). Along the CIFALPS2 profile, the uppermost 20-25 km of the European lower plate consists of a mainly granitic upper crust and associated sedimentary cover (Fig. 2c). To the east of the Jura fold-and-thrust belt, these upper crustal rocks rest on top of a relatively homogeneous lower crust with low *S*-wave velocities, reaching 3.3 km s^{-1} and detected as far east as underneath the Gran Paradiso dome. Such low *S*-wave velocities are not consistent with granulitic rocks of felsic to intermediate composition, which have been suggested for the European lower crust along the CIFALPS profile (Solarino et al., 2018). Instead, they are more consistent with Vs values expected for remnants of the Paleozoic Saxo-Turingian suture zone inherited from the Variscan orogeny (e.g., Guillot et al., 2009b) and later involved in the Alpine orogeny. Notably, smaller volumes of low-Vs rocks at lower-crustal depths are also revealed along the CIFALPS section beneath the Subalpine Chains (Fig. 4e), to the west of a region characterized by felsic-intermediate granulitic rocks. This suggests that relics of this Variscan suture zone are also present to the west of the External massifs, where

they were not previously detected because they are masked by Jurassic-Oligocene sedimentary successions. This Variscan suture zone was possibly involved obliquely into the Western Alps subduction zone, and to a greater extent in the north than in the south, which is consistent with the Variscan paleogeography (Guillot et al., 2009b). Variscan inheritance is also evidenced by the presence of a Moho step detected beneath the Mont Blanc (Fig. 2c) and previously imaged by Lu et al. (2018) and Zhao et al. (2020) in their tomography models. The Moho step is parallel to the surface trace of the Eastern Variscan Shear Zone recognized as a major lithospheric fault active between 320 and 250 Ma (Guillot et al., 2009b) and reactivated during the Alpine orogeny. However, no Variscan inheritance is expected deeper in the mantle.

At depths >40 km beneath the Alpine subduction wedge, the European lower crust is likely eclogitized (Fig. 2c), in line with predicted pressures (>1.2 GPa) and temperatures (>400°C) in that region of the crust, but it is still seismically distinguishable from the underlying mantle lithosphere (Fig. 2d-e) (see Malusà et al., 2021, their Fig. 4, for a review of seismic velocities expected for different rock types under eclogitic facies conditions). No earthquake is associated to this eclogitized lower crust (Eva et al. 2020) because the subduction zone is fossil and has been inactive for a long time. On the western side of the profile, the high Vs (~3.7 km s^{-1}) crust detected from 7-15 km depth beneath the Bresse Graben, and also extending under the western Jura to the east and the Massif Central to the west (Fig. 2c), is likely related to the late Eocene-Oligocene activation of the Cenozoic Rift System of Central Europe (Ziegler, 1992; Sissingh, 2001), which mainly post-dates (U)HP rock exhumation in the Western Alps.

In the northern Western Alps, the eastward-dipping European Moho is located at 25-35 km depth beneath the External zone to the west of the Moho step, reaching ~40 km depth underneath the Frontal Pennine Fault and ~45 km depth beneath the centre of the Gran Paradiso dome. It is less steep than in the southern Western Alps, where the Moho shows a more continuous profile without steps from ~40 km depth beneath the Frontal Pennine Fault to ~70 km depth beneath the core of the Dora-Maira dome (Fig. 4c). A comparison between the CIFALPS2 main profile and the ALP-N and ALPS-S complementary profiles (Fig. 3), located ~20 km to the north and south of the CIFALPS2 main profile, respectively, reveals that the change in European-Moho dip angle takes place over a distance of a few tens of kilometers around the city of Ivrea. To the north of Ivrea (ALP-N profile), the European Moho is quite shallow dipping (Fig. 3c), similarly to what is observed along the CIFALPS2 main profile (Fig. 2c-d). To the south of Ivrea (ALP-S profile), the European Moho is much steeper (Fig. 3g), similarly to what is observed along the CIFALPS profile (Fig. 4c-d).

The eastward-dipping Adriatic Moho is located close to the Earth's surface near Ivrea, and at ~30 km depth farther east, in front of the Monferrato (Fig. 2c). In the Ivrea region, the high-density peridotites of the Adriatic mantle, together with amphibolites of the Sesia-Lanzo unit and lower crustal rocks of the Ivrea-Verbano zone (Scarponi et al., 2020), induce a stronger and narrower Bouguer anomaly than in the south (IGA in Fig. 2a), where the lower but broader positive anomaly (IGA in Fig. 4a) is mostly induced by a deeper (~10 km depth) body of serpentinized mantle rocks located beneath the Dora-Maira dome (SM in Fig. 4c). These observations suggest that the Ivrea gravity anomaly probably has different causes in the northern Western Alps than in the southern Western Alps. The gravity anomalies documented by the pan-Alpine surface-gravity database of Zahorec et al. (2021) also show along-strike variations on the lower-plate side of the orogen (Figs. 2a and 4a). In the External zone of the Western Alps, the negative anomaly is more pronounced along the CIFALPS2 profile (red line in Fig. 2a) than along the CIFALPS profile (grey line in Fig. 2a), while the less steep European Moho would result in a less pronounced negative anomaly in the northern Western Alps than in the southern Western Alps. This negative anomaly matches and possibly reflects the distribution of low-Vs lower-crustal rocks of the previously mentioned Variscan suture zones. Further gravity modelling, which is beyond the aims of this paper, would help confirming such hypothesis and may provide further support to the geologic interpretation of the CIFALPS2 profile shown in Fig. 2c.

The high-velocity seismic body located above interface "3" in Fig. 4e and referred to as "Adria seismic body" by Nouibat et al. (2022), was already detected in the Vp model by Solarino et al. (2018) (Fig. 4f) and included in previous interpretations of the CIFALPS profile. However, the Vs model by Nouibat et al. (2022) allows tracing near-vertical faults located to the east of the Rivoli-Marene Fault down to the lithospheric mantle. These strike-slip faults, like the thrust faults underneath the External massifs, were active for a long time after the exhumation of the subduction wedge (Malusà et al., 2017; Eva et al., 2020). However, the location, attitude and kinematics of these strike-slip faults, and the minor throw accommodated by the thrust faults (see Figs. 2c and 4c), suggest that their impact on the original structure of the subduction wedge is negligible.

The along-strike variations in European-Moho attitude revealed by the CIFALPS experiments have major implications for the structure and evolution of the overlying subduction wedge, which is much smaller in the northern Western Alps (Fig. 2c) than in the southern Western Alps (Fig. 4c). Also, mantle-wedge rocks are less involved in the orogeny in the north than in the south. Along the CIFALPS2 profile, we interpret the set of diffuse negative-polarity

Ps converted phases beneath the Gran Paradiso dome as a progressive velocity change between subducted European crustal rocks and the overlying serpentinized mantle-wedge rocks (Fig. 2c). However, no large body of partly serpentinized mantle-wedge rocks is imaged beneath the Gran Paradiso dome, unlike beneath the Dora-Maira dome. Another major difference is highlighted at the level of the subduction channel, because a thick body of subduction-channel serpentinites and metasomatized mantle peridotites was suggested for the CIFALPS seismic images in the southern Western Alps (Zhao et al., 2020; Malusà et al., 2021), whereas no evidence of a thick and partly exhumed subduction channel has been imaged along the CIFALPS2 profile.

5.2 Lateral Moho variations and relations with the slab structure.

Our analysis reveals that the north-south change in the geometry of the subduction wedge is significant between profiles that are only ~20 km apart. We further investigate the sharpness of this change by mapping the depth of a Moho proxy, that is the iso-velocity surface Vs=4.3 km s^{-1} in Fig. 5a, taking benefit of the 3-D Vs model of Nouibat et al. (2022). According to Figs. 2-4, this surface is a good proxy of the European Moho and a correct proxy for the Adriatic Moho at some distance from the subduction wedge. Close to the subduction wedge, the Adriatic Moho is shallower than the 4.3 km s^{-1} Vs contour, for example because of the serpentinization of upper-mantle peridotites (black dotted area in Fig. 5a). The western boundary of the Adriatic upper plate in the northern Western Alps is marked by the Ivrea gravity anomaly (red dashed line in Fig. 5a).

This Moho proxy depth map highlights the strong and sharp lateral changes in the deep structure of the Western Alps, confirming what is revealed by receiver function analysis (Figs. 2-4). The European Moho reaches very large depth (≥ 70 km, dark blue color in Fig. 5a) almost only in the region between our two profiles, from CIFALPS2 in the north to ~20 km south of CIFALPS in the south. The European Moho is affected by a major step, outlined by purple arrows in Fig. 5a, which is almost aligned with the Mont Blanc and Belledonne external massifs. The yellow arrows mark instead the region with the strongest along-strike change in European Moho attitude, which is located to the south of the Gran Paradiso dome and oriented ENE-WSW. The shallow body of Vs >4.3 km s^{-1} (yellow star in Fig. 5a) that is crosscut by the CIFALPS profile and interpreted as dry Adriatic mantle in Fig. 3c, has a very small size of ~20 × 40 km^2 and is exclusively located to the east of the Dora-Maira dome, within the region showing the deepest European Moho. This high-velocity body is clearly crosscut, in map view, by the Rivoli-Marene Fault (RMF in Fig. 5a), which marks the western boundary of the Adriatic

upper plate in the southern Western Alps, in agreement with the interpretive geologic cross-section of Fig. 3c.

The ENE-WSW change in European Moho attitude shown in the map, when plotted on a 100-km depth slice of the *P*-wave velocity perturbation model of Zhao et al. (2016b) (black arrows in Fig. 5b) is aligned with a major bend in the high velocity anomaly interpreted as the European slab (dark blue colors in Fig. 5b). This suggests that the observed depression in the European Moho could be a response to slab bending, which was likely promoted by the Cenozoic northward motion and indentation of the Adriatic upper plate before (U)HP rock exhumation (Fig. 5c). We exclude any potential change in European Moho attitude either due to European slab breakoff or European slab rollback after (U)HP rock exhumation. Recent tomography models of the Alpine region document in fact a continuous and undetached European slab beneath the Western Alps down to the mantle transition zone (e.g., Zhao et al., 2016b; Rappisi et al., 2022), whereas late-stage slab rollback would imply an additional exhumation event on the lower-plate side of the orogen, which is not observed (Malusà et al., 2015).

5.3 Implications for (U)HP rock exhumation

An effective application of our findings for a better understanding of continental subduction and exhumation requires a reliable knowledge of structures and geometries that are preserved since the time of (U)HP rock exhumation. Structures formed at a later stage should be retro-deformed or excluded. The latter include the thrust faults detected underneath the External massifs along the CIFALPS2 transect, and the strike-slip faults cutting across the Adriatic lithosphere along the CIFALPS transect. The complex 3-D tectonic structure of the fossil subduction wedge and the European Moho, and their sharp north-south variations, are instead substantially preserved since 30 Ma.

We speculate that in the European lithosphere, the presence of remnants of older suture zones involved obliquely by Alpine subduction, and to a greater extent in the north than in the south, may have favoured the development of a shallower-dipping Moho in the northern Western Alps than in the southern Western Alps. These lateral variations should be considered in conceiving the next-generation thermo-mechanical numerical models. Because they were already present during subduction, they may have affected the prograde pressure-temperature-time path recorded by (U)HP rocks now exposed at the Earth's surface. In fact, a deeper subduction angle implies a faster burial path if the convergence rates remain the same. The sharp change in Moho attitude was likely emphasized during northward motion of Adria, thus

preparing an even more laterally variable tectonic framework for the subsequent exhumation stage.

During (U)HP rock exhumation, the tectonic framework was largely controlled by the indentation of Adriatic lithosphere beneath the Central Alps, and the consequent transtension in the Western Alps (Fig. 5c) coeval to the activity of lithospheric strike-slip structures. Even though the divergent component of plate motion along the Western Alpine subduction zone increased quite progressively from north to south, the underlying lower-plate structure was characterized by sharp changes along strike. This provided much more space available for (U)HP rock exhumation in the south than in the north. As a result, the subduction wedge is much thicker in the southern Western Alps, along the Dora-Maira transect than in the northern Western Alps along the Gran Paradiso transect (e.g., Liao et al., 2018). Mantle-wedge rocks are deeply involved in orogeny exclusively in the south, where exhumation processes also involve the deepest levels of the Western Alps subduction channel (Zhao et al., 2020; Malusà et al., 2021). Moreover, coesite-bearing continental rocks are exclusively found in the south, in several localities of the Dora-Maira massif (black diamonds in Fig. 5a), but not in the north. We conclude that lateral variations in exhumation style revealed by the geologic record are potentially controlled by sharp changes in the deep tectonic structure that can be only revealed by cutting-edge geophysical analyses.

6. Conclusions

The new receiver function cross-sections of the CIFALPS2 and CIFALPS seismic experiments in the Western Alps, supported by a 3-D shear-wave velocity model, provide evidence for a marked change in European Moho attitude from the northern to the southern Western Alps, taking place over a distance of a few tens of kilometers. This sharp change was likely favored by involvement of remnants of Variscan suture zones in the Alpine subduction zone, and was later emphasized by slab deformation during subduction, prior to (U)HP rock exhumation. Our study reveals a much thicker subduction wedge in the southern Western Alps than in the northern Western Alps. Mantle-wedge rocks were deeply involved in orogeny exclusively in the southern Western Alps, where exhumation processes also involve deep levels of the subduction channel, and where coesite-bearing continental rocks are exhumed to the Earth's surface. This detailed information on the 3-D structure of the Alpine subduction wedge provides first-order constraints for next-generation 3-D thermo-mechanical numerical models. The resulting picture underlines the importance of lateral variations in the dip angle of the lower

plate during scissor-type divergent motion of the upper plate, which may lead to the exhumation of larger volumes of (U)HP rocks in specific sites of the subduction zone.

Acknowledgements

This research is funded by the National Natural Science Foundation of China (grants 41625016, 41888101, and 91955210), the Agence Nationale de la Recherche (France; AlpArray-FR project, contract ANR-15-CE31-0015), LabEx OSUG@2020 (Investissements d'Avenir, ANR-10-LABX-56) and by the Référentiel Géologique de la France program (RGF, http://rgf.brgm.fr/). We are grateful to the many individuals and municipalities who helped us finding good sites for our temporary stations and who hosted them. We also thank all our colleagues and students who participated in the field work. AP warmly thanks Florian Millet for sharing his receiver function processing software package. Chris Beaumont and an anonymous reviewer provided insightful comments that helped improve an initial version of the paper.

Data availability

Seismic data of the CIFALPS (doi:10.15778/RESIF.YP2012) and CIFALPS2 (doi:10.15778/RESIF.XT2018) temporary experiments are archived and distributed by the datacenter of the French geodetic and seismological network RESIF, which is an EIDA node (European Integrated Data Archive), and by the IGGCAS datacenter (Institute of Geology and Geophysics, Chinese Academy of Sciences). We also used records of permanent networks CH (doi:10.12686/sed/networks/ch), GU (doi:10.7914/SN/GU), IV (doi:10.13127/SD/X0FXnH7QfY), FR (doi:10.15778/RESIF.FR), and of the AlpArray seismic network Z3 (doi:10.12686/alparray/z3_2015). The shear-wave velocity model of Nouibat et al. (2022) will be distributed by the RESIF data repository (https://www.resif.fr/donnees-et-produits/entrepot-produits/#/), or is available upon request to the first author.

Author contributions

Anne Paul: conceptualization, funding acquisition, project administration, methodology, investigation, data curation, formal analysis, visualization, writing - original draft. **Marco G. Malusà**: conceptualization, investigation, visualization, writing - original draft. **Stefano Solarino**: conceptualization, project administration, investigation, data curation, writing - review and editing. **Simone Salimbeni**: conceptualization, investigation, data curation, writing

- review and editing. **Elena Eva**: conceptualization, investigation, data curation, writing - review and editing. **Ahmed Nouibat**: methodology, formal analysis, writing - review and editing. **Silvia Pondrelli**: conceptualization, investigation, data curation, writing - review and editing. **Coralie Aubert**: investigation, data curation, writing - review and editing. **Thierry Dumont**: conceptualization, visualization, writing - review and editing. **Stéphane Guillot**: conceptualization, writing - review and editing. **Stéphane Schwartz**: conceptualization, visualization, writing - review and editing. **Liang Zhao**: conceptualization, funding acquisition, project administration, investigation, writing - review and editing.

References

Alder, C., Debayle, E., Bodin, T., Paul, A., Stehly, L., Pedersen, H., & AlpArray Working Group. (2021). Evidence for radial anisotropy in the lower crust of the Apennines from Bayesian ambient noise tomography in Europe. Geophysical Journal International, 226(2), 941-967.

AlpArray Seismic Network, 2015. AlpArray Seismic Network (AASN) temporary component. AlpArray Working Group. doi:10.12686/alparray/z3_2015

Beller, S., Monteiller, V., Operto, S., Nolet, G., Paul, A., & Zhao, L., 2018. Lithospheric architecture of the South-Western Alps revealed by multiparameter teleseismic full-waveform inversion. Geophysical Journal International, 212(2), 1369-1388.

Bigi, G., Cosentino, D., Parotto, M., Sartori, R., & Scandone, P., 1990. Structural model of Italy and gravity map. Sheets 1-9, 1:500.000. Progetto Finalizzato Geodinamica C.N.R. Quaderni Ricerca Scientifica, 114 (3).

Butler, J. P., Beaumont, C., & Jamieson, R. A., 2013. The Alps 1: A working geodynamic model for burial and exhumation of (ultra-) high-pressure rocks in Alpine-type orogens. Earth and Planetary Science Letters, 377, 114-131.

Cassano, E., Anelli, L., Fichera, R., & Cappelli, V., 1986. Pianura Padana, interpretazione integrata di dati geofisici e geologici, AGIP Servizi Centrali per l'Esplorazione, Metodologie e Appl. Geofisiche, Milano, 28.

Chopin, C., 1984. Coesite and pure pyrope in high-grade blueschists of the Western Alps: a first record and some consequences. Contributions to Mineralogy and Petrology, 86(2), 107-118.

Dal Piaz, G. V., 2001. History of tectonic interpretations of the Alps. Journal of geodynamics, 32(1-2), 99-114.

Dueker, K. G., & Sheehan, A. F., 1997. Mantle discontinuity structure from midpoint stacks of converted P to S waves across the Yellowstone hotspot track. Journal of Geophysical Research: Solid Earth, 102(B4), 8313-8327.

Dumont, T., Schwartz, S., Guillot, S., Malusà, M., Jouvent, M., Monié, P., & Verly, A. (2022). Cross-propagation of the western Alpine orogen from early to late deformation stages: Evidence from the Internal Zones and implications for restoration. Earth-Science Reviews, 104106.

ECORS-CROP DSS Group, 1989. A new picture of the Moho under the western Alps. Nature 337, 249-251.

Eva, E., Malusà, M. G., & Solarino, S., 2020. Seismotectonics at the transition between opposite-dipping slabs (western Alpine region). Tectonics, 39(9), e2020TC006086.

Guillot, S., di Paola, S., Ménot, R. P., Ledru, P., Spalla, M. I., Gosso, G., & Schwartz, S., 2009a. Suture zones and importance of strike-slip faulting for Variscan geodynamic reconstructions of the External Crystalline Massifs of the western Alps. Bulletin de la Société géologique de France, 180(6), 483-500.

Guillot, S., Hattori, K., Agard, P., Schwartz, S., & Vidal, O., 2009b. Exhumation processes in oceanic and continental subduction contexts: a review. Subduction zone geodynamics, 175-205.13.

Handy, M. R., Schmid, S. M., Bousquet, R., Kissling, E., & Bernoulli, D., 2010. Reconciling plate-tectonic reconstructions of Alpine Tethys with the geological–geophysical record of spreading and subduction in the Alps. Earth-Science Reviews, 102(3-4), 121-158.

INGV Seismological Data Centre, 2006. Rete Sismica Nazionale (RSN). Istituto Nazionale di Geofisica e Vulcanologia (INGV), Italy. doi:10.13127/SD/X0FXnH7QfY

Kennett, B. L. N., & Engdahl, E. R., 1991. Traveltimes for global earthquake location and phase identification. Geophysical Journal International, 105(2), 429-465.

Langston, C. A., 1979. Structure under Mount Rainier, Washington, inferred from teleseismic body waves. Journal of Geophysical Research: Solid Earth, 84(B9), 4749-4762.

Liao, J., Malusà, M. G., Zhao, L., Baldwin, S. L., Fitzgerald, P. G., & Gerya, T., 2018. Divergent plate motion drives rapid exhumation of (ultra) high pressure rocks. Earth and Planetary Science Letters, 491, 67-80.

Lu, Y., Stehly, L., Paul, A., & AlpArray Working Group, 2018. High-resolution surface wave tomography of the European crust and uppermost mantle from ambient seismic noise. Geophysical Journal International, 214(2), 1136-1150.

Malusà, M. G., Faccenna, C., Garzanti, E., & Polino, R., 2011. Divergence in subduction zones and exhumation of high pressure rocks (Eocene Western Alps). Earth and Planetary Science Letters, 310(1-2), 21-32.

Malusà, M. G., Faccenna, C., Baldwin, S. L., Fitzgerald, P. G., Rossetti, F., Balestrieri, M. L., Danišík, M., Ellero, A., Ottria, G., and Piromallo, C., 2015. Contrasting styles of (U)HP rock exhumation along the Cenozoic Adria-Europe plate boundary (Western Alps, Calabria, Corsica). Geochemistry, Geophysics, Geosystems, 16(6), 1786-1824.

Malusà, M. G., Zhao, L., Eva, E., Solarino, S., Paul, A., Guillot, S., Schwartz, S., Dumont, T., Aubert, C., Salimbeni, S., Pondrelli, S., Wang, Q., & Zhu, R., 2017. Earthquakes in the western Alpine mantle wedge. Gondwana Research, 44, 89-95.

Malusà, M. G., Guillot, S., Zhao, L., Paul, A., Solarino, S., Dumont, T., Schwartz, S., Aubert, C., Baccheschi, P., Eva, E., Lu, Y., Lyu, C., Pondrelli, S., Salimbeni, S., Sun, W., & Yuan, H., 2021. The deep structure of the Alps based on the CIFALPS seismic experiment: A synthesis. Geochemistry, Geophysics, Geosystems, 22(3), e2020GC009466.

Manzotti, P., Schiavi, F., Nosenzo, F., Pitra, P., & Ballèvre, M. (2022). A journey towards the forbidden zone: a new, cold, UHP unit in the Dora-Maira Massif (Western Alps). Contributions to Mineralogy and Petrology, 177(6), 1-22.

Millet, F., Bodin, T., & Rondenay, S., 2019. Multimode 3-D Kirchhoff migration of receiver functions at continental scale. Journal of Geophysical Research: Solid Earth, 124(8), 8953-8980.

Nicolas, A., Hirn, A., Nicolich, R., & Polino, R., 1990. Lithospheric wedging in the western Alps inferred from the ECORS-CROP traverse. Geology, 18(7), 587-590.

Nouibat, A., Stehly, L., Paul, A., Schwartz, S., Bodin, T., Dumont, T., Rolland, Y., Brossier, R., Cifalps Team & AlpArray Working Group, 2022. Lithospheric transdimensional ambient-noise tomography of W-Europe: implications for crustal-scale geometry of the W-Alps. Geophysical Journal International, 229(2), 862-879.

Pfiffner, O. A., Schlunegger, F., & Buiter, S. J. H., 2002. The Swiss Alps and their peripheral foreland basin: Stratigraphic response to deep crustal processes. Tectonics, 21(2), 3-1.

Rappisi, F., VanderBeek, B. P., Faccenda, M., Morelli, A., & Molinari, I. (2022). Slab Geometry and Upper Mantle Flow Patterns in the Central Mediterranean From 3D Anisotropic P-Wave Tomography. Journal of Geophysical Research: Solid Earth, 127(5), e2021JB023488.

RESIF, 1995. RESIF-RLBP French Broad-band network, RESIF-RAP strong motion network and other seismic stations in metropolitan France [Data set]. RESIF - Réseau Sismologique et géodésique Français. doi:10.15778/RESIF.FR

Rondenay, S., 2009. Upper mantle imaging with array recordings of converted and scattered teleseismic waves. Surveys in geophysics, 30(4), 377-405.

Roure, F., Polino, R., & Nicolich, R., 1990. Early Neogene deformation beneath the Po Plain: constraints on the post-collisional Alpine evolution: Mémoires Société Géologique de France, v. 156.

Salimbeni, S., Piana Agostinetti, N., Pondrelli, S., & CIFALPS Working Group. (2021). Insights into the origin and deformation style of the continental Moho: A case-study from the Western Alps (Italy). Journal of Geophysical Research: Solid Earth, 126(6), e2020JB021319.

Scarponi, M., Hetényi, G., Berthet, T., Baron, L., Manzotti, P., Petri, B., Pistone, M., & Müntener, O., 2020. New gravity data and 3-D density model constraints on the Ivrea Geophysical Body (Western Alps). Geophysical Journal International, 222(3), 1977-1991.

Sénéchal, G., & Thouvenot, F., 1991. Geometrical migration of line-drawings: A simplified method applied to Ecors data. Continental Lithosphere: Deep Seismic Reflections, Geodynamics Series 22, American Geophysical Union, 401-407.

Sissingh, W., 2001. Tectonostratigraphy of the West Alpine Foreland: correlation of Tertiary sedimentary sequences, changes in eustatic sea-level and stress regimes. Tectonophysics, 333(3-4), 361-400.

Solarino, S., Malusà, M. G., Eva, E., Guillot, S., Paul, A., Zhao, L., Aubert, C., Dumont, T., Pondrelli, S., Salimbeni, S., Schwartz, S., Wang, Q., Xu, X., Zheng, T., & Zhu, R., 2018. Mantle wedge exhumation beneath the Dora-Maira (U)HP dome unravelled by local earthquake tomography (Western Alps). Lithos, 296, 623-636.

Swiss Seismological Service (SED) At ETH Zurich, 1983. National Seismic Networks of Switzerland. ETH Zürich. doi:10.12686/sed/networks/ch

University of Genoa, 1967. Regional Seismic Network of North Western Italy [Data set]. International Federation of Digital Seismograph Networks. doi:10.7914/SN/GU

Vinnik, L. P., 1977. Detection of waves converted from P to SV in the mantle. Physics of the Earth and planetary interiors, 15(1), 39-45.

Webb, L. E., Baldwin, S. L., Little, T. A., & Fitzgerald, P. G., 2008. Can microplate rotation drive subduction inversion? Geology, 36(10), 823-826.

Yamato, P., Burov, E., Agard, P., Le Pourhiet, L., & Jolivet, L., 2008. HP-UHP exhumation during slow continental subduction: Self-consistent thermodynamically and thermomechanically coupled model with application to the Western Alps. Earth and Planetary Science Letters, 271(1-4), 63-74.

Zahorec, P., Papčo, J., Pašteka, R., Bielik, M., Bonvalot, S., Braitenberg, C., et al., 2021. The first pan-Alpine surface-gravity database, a modern compilation that crosses frontiers. Earth System Science Data, 13(5), 2165-2209.

Zhao, L., Paul, A., Guillot, S., Solarino, S., Malusà, M. G., Zheng, T.Y., Aubert, C., Salimbeni, S., Dumont, T., Schwartz, S., Zhu, R.X., & Wang, Q.C., 2015. First seismic evidence for continental subduction beneath the Western Alps. Geology, 43(9), 815-818.

Zhao, L., Paul, A., Solarino, S., & RESIF, 2016a. Seismic network YP: CIFALPS temporary experiment (China-Italy-France Alps seismic transect) [Data set]. RESIF - Réseau Sismologique et géodésique Français. doi:10.15778/RESIF.YP2012

Zhao, L., Paul, A., Malusà, M. G., Xu, X., Zheng, T., Solarino, S., Guillot, S., Schwartz, S., Dumont, T., Salimbeni, S., Aubert, C., Pondrelli, S., Wang, Q., & Zhu, R., 2016b. Continuity of the Alpine slab unraveled by high-resolution P wave tomography. Journal of Geophysical Research: Solid Earth, 121(12), 8720-8737.

Zhao, L., A. Paul, S. Solarino, RESIF, 2018. Seismic network XT: CIFALPS2 temporary experiment (China-Italy-France Alps seismic transect #2). RESIF - Réseau Sismologique et géodésique Français. doi:10.15778/resif.xt2018

Zhao, L., M.G. Malusà, H. Yuan, A. Paul, S. Guillot, Y. Lu, S. Solarino, E. Eva, G. Lu, T. Bodin, Cifalps Group, AlpArray Working Group, 2020. Evidence for a serpentinized plate interface favouring continental subduction. Nature communications, 11(1), 1-8.

Ziegler, P. A., 1992. European Cenozoic rift system. Tectonophysics, 208(1-3), 91-111.

FIGURE 1

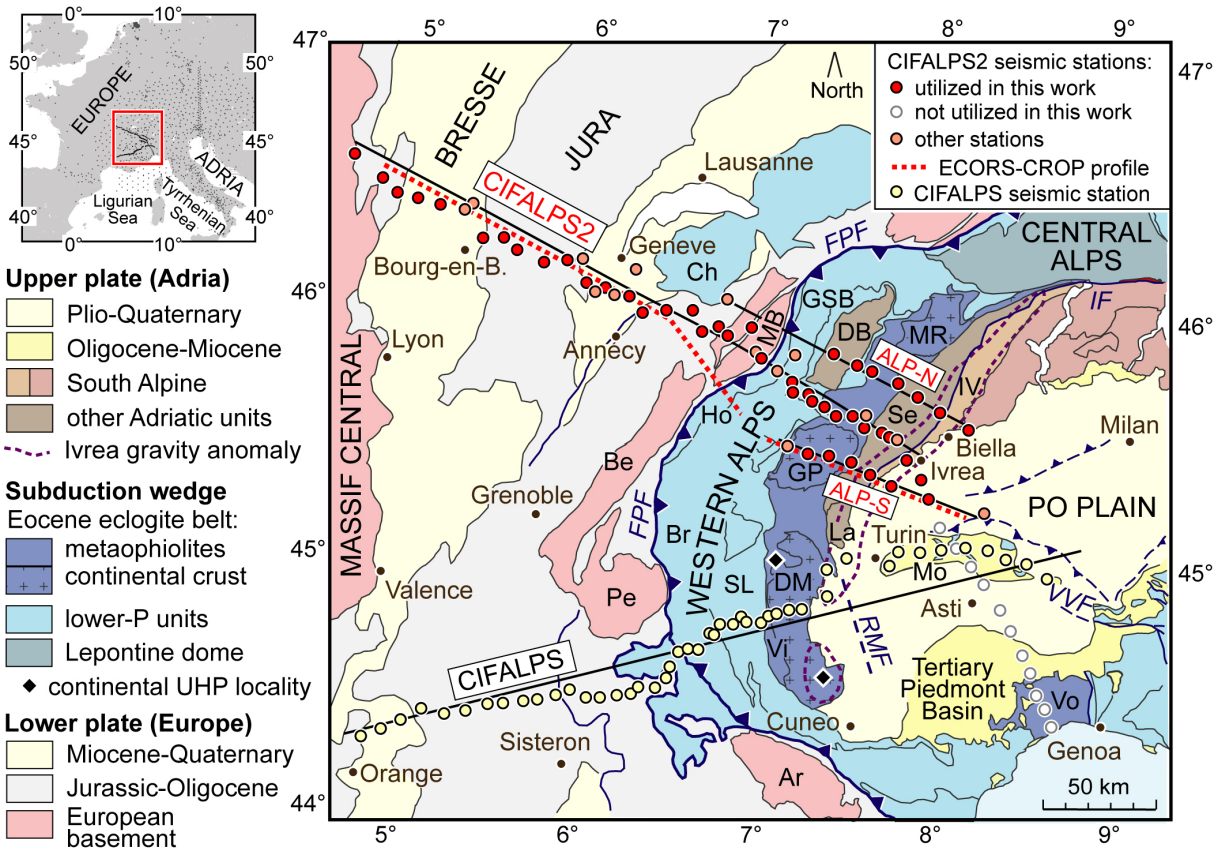

Figure 1: Locations of the CIFALPS temporary seismic experiments across the Western Alps. The thick black lines in the map (modified after Malusà et al., 2015) indicate the profiles of Figs. 2, 3 and 4 (ALP-N and ALP-S are the complementary profiles of the CIFALPS2 experiment). The pink dots are seismic stations from other networks used in the receiver function study. The purple dashed line is the 0-mGal contour of the Ivrea gravity anomaly (from Bigi et al., 1990). The dotted red line shows the location of the ECORS-CROP deep seismic sounding reflection section. The grey dots in the top-left inset indicate the seismic stations used in the ambient-noise tomography of Nouibat et al. (2022). Acronyms: Ar, Argentera; Be, Belledonne; Br, Briançonnais; Ch, Chablais; DB, Dent Blanche; DM, Dora-Maira; FPF, Frontal Pennine Fault; GP, Gran Paradiso; GSB, Grand St-Bernard; Ho, Houiller; IF, Insubric Fault; IV, Ivrea-Verbano; La, Lanzo; MB, Mont Blanc; MR, Monte Rosa; Pe, Pelvoux; RMF, Rivoli-Marene Fault; Se, Sesia-Lanzo; SL, Schistes lustrés; Vi, Viso; Vo, Voltri; VVF, Villalvernia-Varzi Fault. Continental UHP localities (black diamonds) after Chopin (1984) and Manzotti et al. (2022).

FIGURE 2

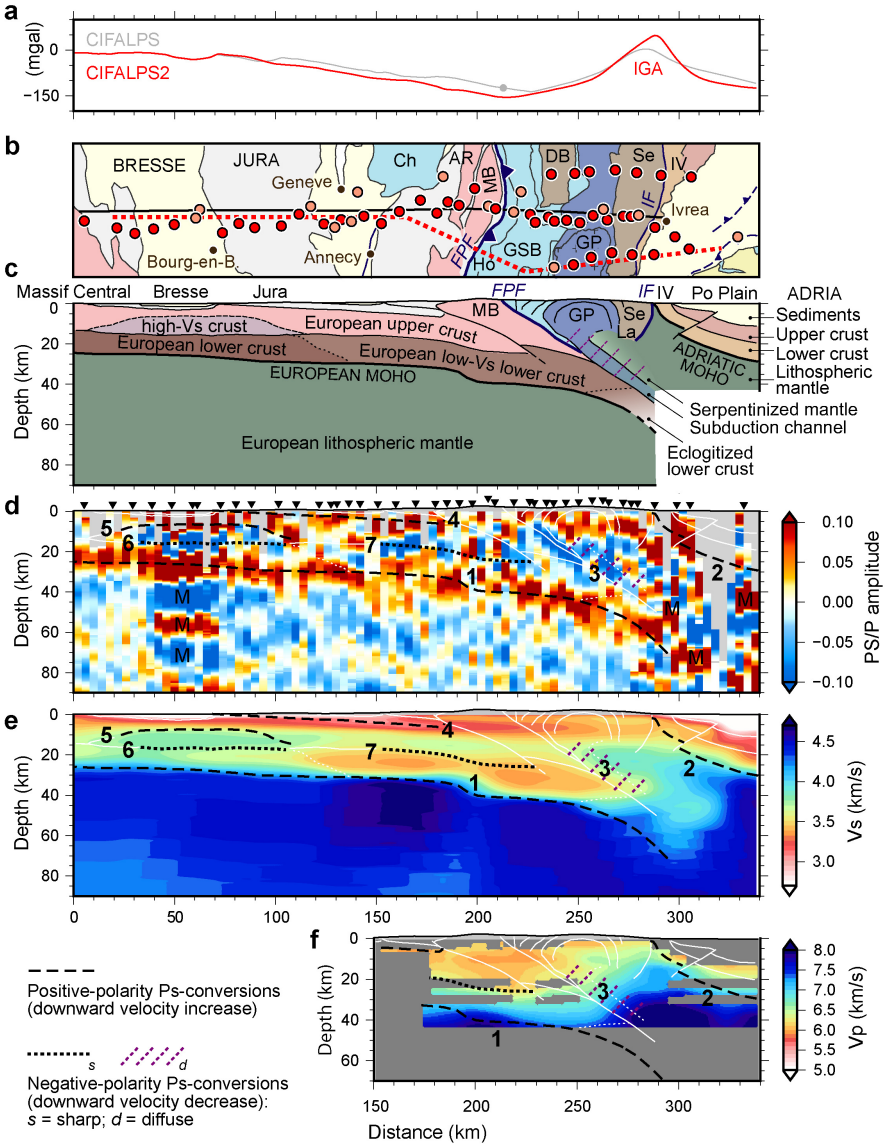

Figure 2: Depth sections along the CIFALPS2 main profile across the northern Western Alps. a: Bouguer anomaly from the gravity database of Zahorec et al. (2021) (in red); IGA: Ivrea gravity anomaly. The Bouguer anomaly along the CIFALPS profile is shown for comparison (in grey; the grey dot indicates the Frontal Pennine Fault). **b:** Geological map around the main profile (black line), see Fig. 1 for location and acronyms. **c:** Interpretive geologic cross-section. **d:** CCP stacked section for teleseismic earthquakes of 0-100° back-azimuth, with labels and dashed black lines (for positive-polarity Ps conversions and downward velocity decrease) or dotted black or purple lines (for negative-polarity Ps conversions and downward velocity increase) outlining the main features discussed in the text (labels 1-7). M: multiples. **e:** Vs section from Nouibat et al. (2022) used for time-to-depth migration of the CCP stack (Vp/Vs = 1.8). **f:** Vp section from the local earthquake tomography of Solarino et al. (2018). Note the consistency between interfaces identified by independent methods in (d) and (e).

FIGURE 3

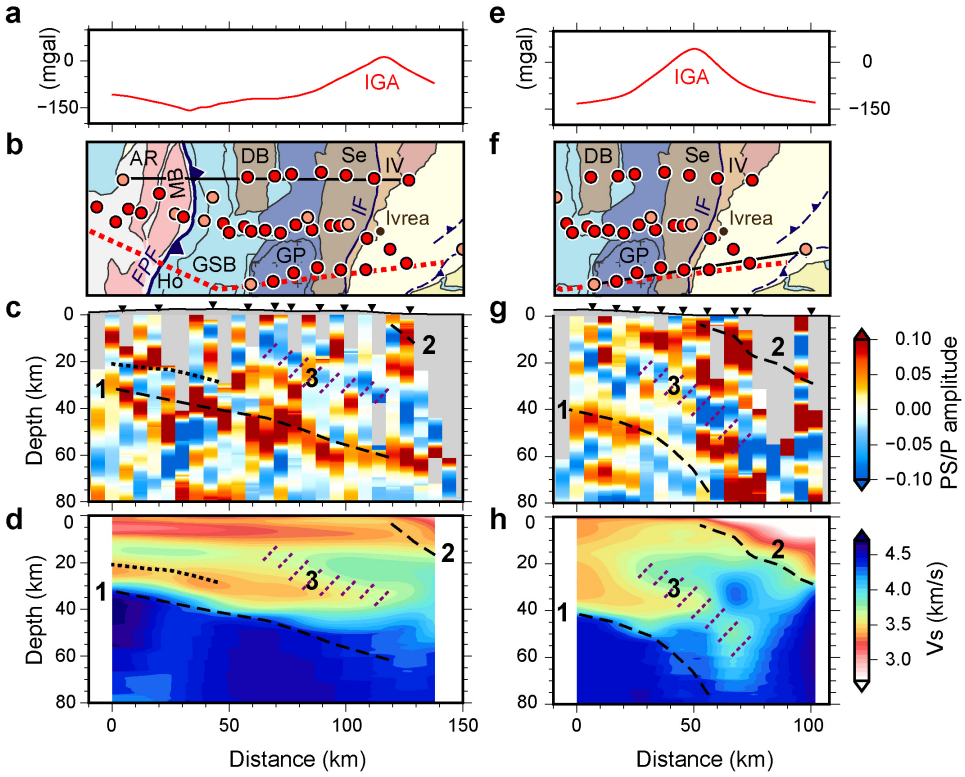

Figure 3: Depth sections along the ALP-N (left) and ALP-S (right) complementary profiles (same keys as Fig. 2). **a, e:** Bouguer anomaly (Zahorec et al., 2021). **b, f:** Geological map. **c, g:** CCP receiver-function stack (computed with Vp/Vs=1.8). **d, h:** Vs section (Nouibat et al., 2022). Labels 1-3 indicate regions discussed in the text. Note the consistency between interfaces identified by independent methods in (c), (d) and (g), (h).

FIGURE 4

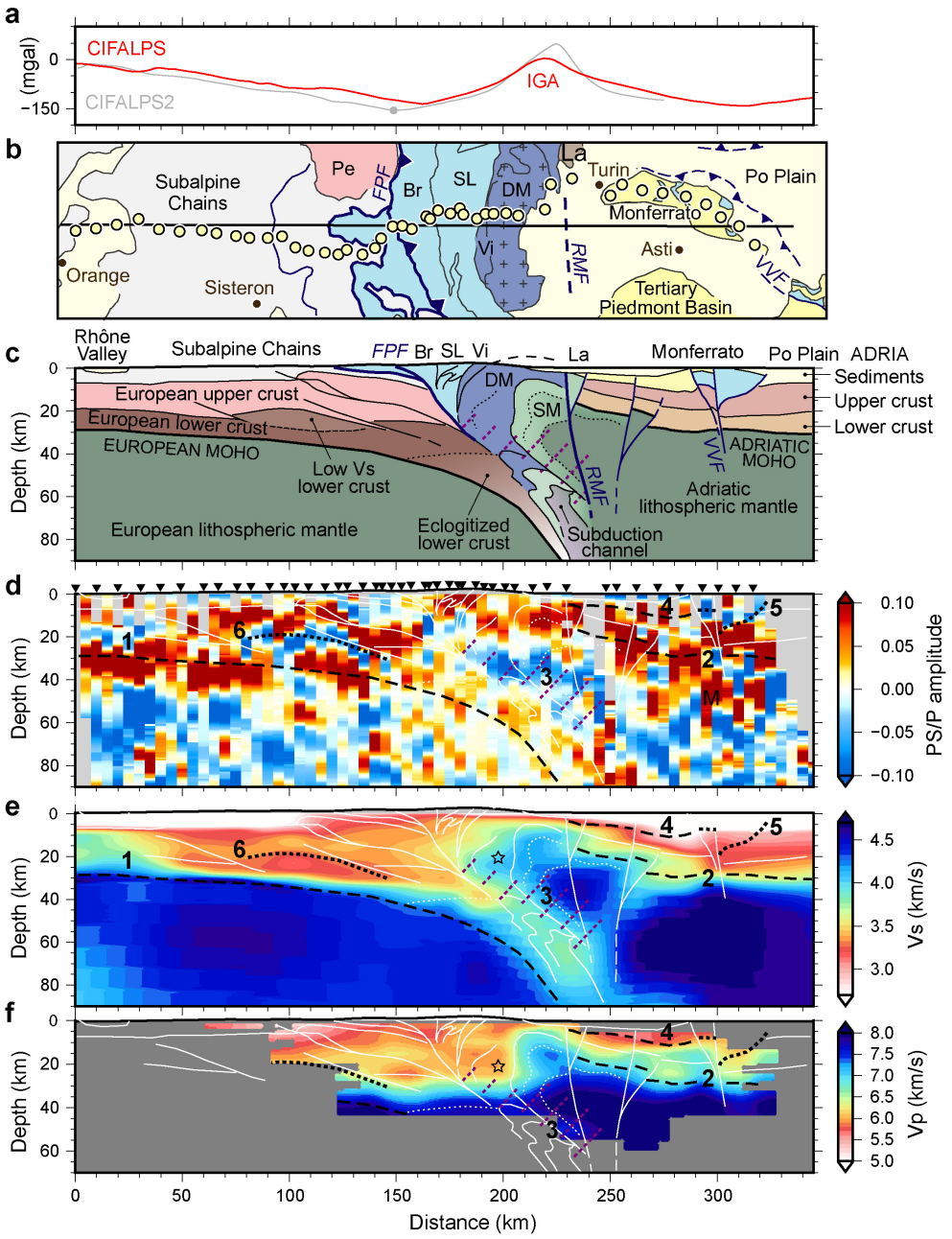

Figure 4: Depth sections along the CIFALPS profile across the southern Western Alps (same keys as Fig. 2). **a:** Bouguer anomaly (Zahorec et al., 2021) (in red). The Bouguer anomaly along the CIFALPS2 profile is shown for comparison (in grey; the grey dot indicates the Frontal Pennine Fault). **b:** Geological map. **c:** Interpretive geologic cross-section (modified after Malusà et al., 2021); **d:** CCP receiver-function stack (computed with Vp/Vs=1.7). **e:** Vs section (Nouibat et al., 2022). **f:** Vp section (Solarino et al., 2018). Labels 1-6 and the region marked by a star are discussed in the text. Note the consistency between interfaces identified by independent methods in (d) and (e).

FIGURE 5

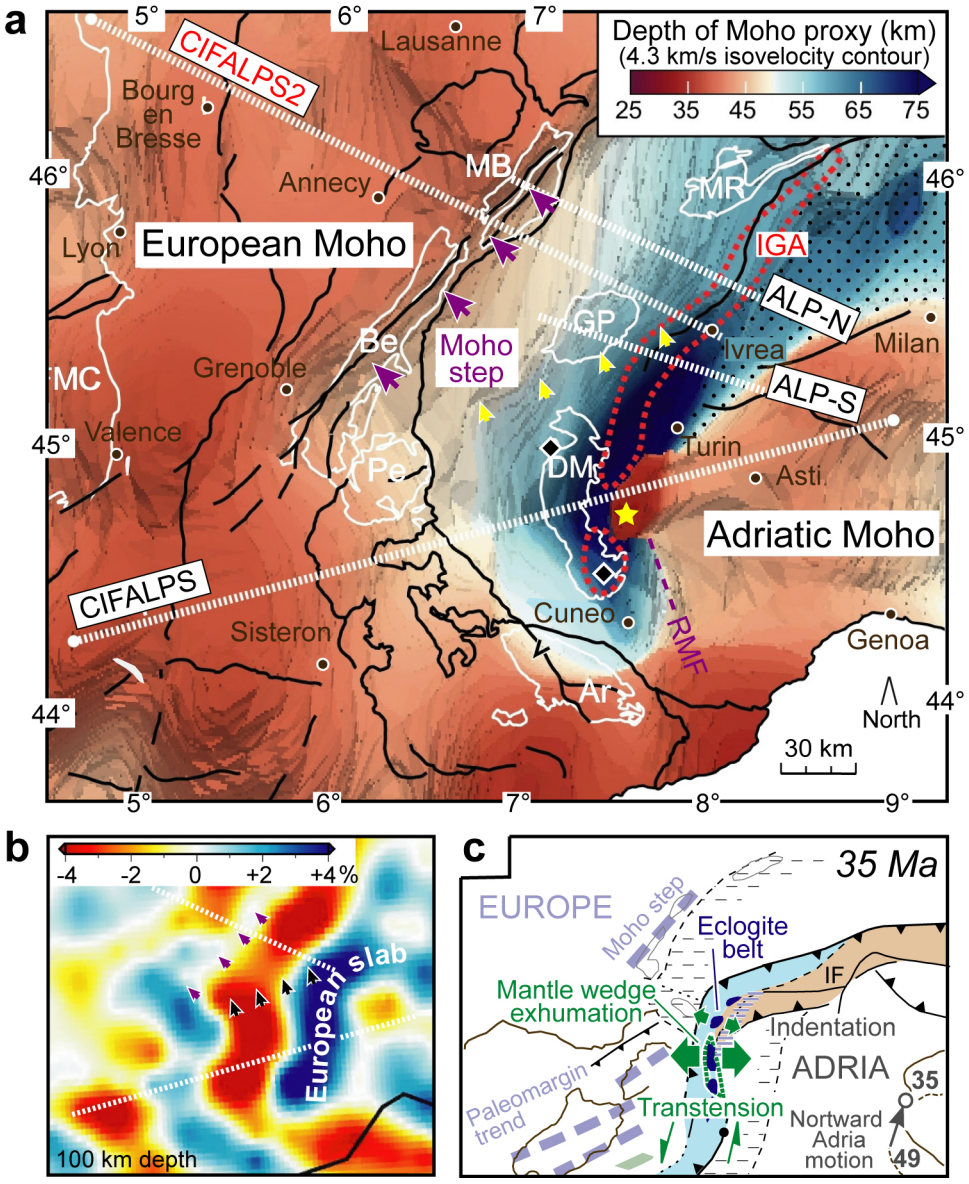

Figure 5: Along-strike Moho variations and relations with the slab structure. a: Analyzed profiles on a Moho-proxy depth map based on the S-wave velocity model by Nouibat et al. (2022), where the iso-velocity surface Vs=4.3 km/s is considered as the best proxy for the European Moho. Geologic boundaries (thin white lines) and major faults (black lines) are also shown for reference (same acronyms as Fig. 1; MC: Massif Central). Black dots mark the area where the Adriatic Moho lays at shallower levels than Vs=4.3 km/s (e.g., due to serpentinization of the uppermost mantle, see main text and Figs. 2, 3 and 4 for details). Purple arrows: inherited Moho step in the lower plate (Lu et al., 2018). Yellow arrows: region with the strongest along-strike change in Moho attitude. Yellow star: mantle-lithosphere dry peridotite at shallow depth. Black diamonds: continental UHP localities (Chopin, 1984; Manzotti et al., 2022). Dotted red line: 0-mGal contour of the Ivrea gravity anomaly (IGA, from Bigi et al. 1990). **b:** Upper mantle

depth slice of the P-wave velocity perturbation model of Zhao et al. (2016a) (depth 100 km; same region as (a)). The strongest along-strike change in Moho attitude (black arrows) is aligned with a major bend in the European slab (dark blue colors in the model). **c:** Palinspastic reconstruction of the Alpine subduction zone at 35 Ma, showing the indentation of Adriatic lithosphere in the Central Alps and consequent transtension in the Western Alps leading to (U)HP rock and mantle-wedge exhumation. The exhumed mantle wedge of the southern Western Alps (in green) is juxtaposed against previously exhumed mantle rocks at the tip of the Adriatic upper plate (horizontal lilac lines). The grey arrow indicates Adria-Europe relative plate motion (after Malusà et al., 2021).

Supplementary material

Along-strike variations in the fossil subduction zone of the Western Alps revealed by the CIFALPS seismic experiments and their implications for exhumation of (ultra-) high-pressure rocks

A. Paul [1], M.G. Malusà [2], S. Solarino [3], S. Salimbeni [4], E. Eva [3], A. Nouibat [1], S. Pondrelli [4], C. Aubert [1], T. Dumont [1], S. Guillot [1], S. Schwartz [1], L. Zhao[5]

Content :

S1- Technical strategy used in the CIFALPS2 temporary seismic experiment

Although the CIFALPS and CIFALPS2 experiments were dense profiles (average spacing 5-10 km) with durations of 13-14 months, we applied similar technical strategies as for 2-D arrays with station spacing > 50 km deployed for 2-3 years such as AlpArray. Indeed, most stations had very broadband (BB) velocimeters with flat response in the 8 mHz – 100 Hz band (mostly Nanometrics Trillium Horizon for CIFALPS2), which justified a careful installation to ensure optimal quality recordings. The vault type designed for the CIFALPS experiment (2012-2013) was used as an example in the technical strategy document of the AlpArray seismic network (AlpArray_TechnicalStrategy.pdf). It was further improved for CIFALPS2 (2018-2020) to optimize the thermal protection of the sensor while keeping a cost-effective and manageable workload with two-person field teams.

Fifty instruments of the CIFALPS2 experiment were Trillium Horizon BB velocimeters with mostly Centaur and a few Taurus data acquisition systems (DAS) belonging to the IGG-CAS pool of mobile seismic instruments. The RESIF-SISMOB French national pool of mobile instruments provided five additional instruments with Güralp CMG40T and Nanometrics Centaur DASs. These five instruments were installed at the most remote sites in the Gran Paradiso massif for a longer time period (2 yrs) to ensure optimal data recovery at sites that were difficult or impossible to access in winter, but important for scientific objectives.

The 55 sites were carefully selected, inside unused buildings and with access to mains power when possible. Only 11 stations had solar panels. 52 stations had 3G modems, the other three being located in no-coverage zones. State-of-health parameters of the telemetered Trillium Centaur data acquisition systems were continuously monitored using the SyNApSE web interface developed for the RESIF French national permanent broadband network. Data were transmitted in real time to the RESIF-DC real time server in Grenoble using the seedlink protocol. They were processed (metadata construction, checking and filling of data holes, SDS archive formatting) by the RESIF-DC data processing server. They were then archived and distributed to project participants after a latency of 2-3 days by the RESIF EIDA node using standard distribution tools (rsync, webservices). For more information on the RESIF data information system, we refer to Pequegnat et al. (2021).

The 98% data availability rate (averaged over the time period July 2018 - Feb. 2020) is outstanding for this type of reasonable cost experiment in a mountain environment. Most data loss is related to offline stations and/or solar panels problems.

Fig. S1 shows probability density functions (PDF) of power spectral densities (PSD, McNamara & Buland, 2004) of two representative stations of CIFALPS2. They were computed using the PQLX software (IRIS-PASSCAL Quick Look extended; McNamara & Boaz, 2011) implemented in the RESIF datacenter to evaluate seismic station performance and check instrument responses. Station CI15 (XT.CI15; Fig. S1a) is located in a monastery in the French Alps (Le Reposoir, Haute-Savoie, elevation 1111m), therefore in a very quiet environment. The station performs well with respect to noise level on the vertical component, with PDFs close to the low-noise model (NLNM; Peterson, 1993) at periods > 10s and ~30 dB below the high-noise model (NLHM) at shorter periods. As usual, the PSDs of the horizontal components show higher noise levels than the vertical at long periods (>30s), but still lower than the NLHM in the whole period band. Station CI33 (XT.CI33) is located in Mazzè (Piemonte, Italy, elevation 294m), ~20 km south of the city of Ivrea. It is the most eastward CIFALPS2 station that we used in the receiver function profiles. It is located in the foothills very close to the Po basin, which is a nightmare for seismologists due to very soft soil and high anthropic noise level. Station CI33 performs as well as CI15 at periods >10s. Its noise level is closer to the NLHM at short periods, but still below it, which is a very good result.

The CIFALPS2 (XT) dataset is archived and distributed by the RESIF EIDA node (doi:10.15778/resif.xt2018). It will become public three years after the end of the experiment, on 1 July 2023.

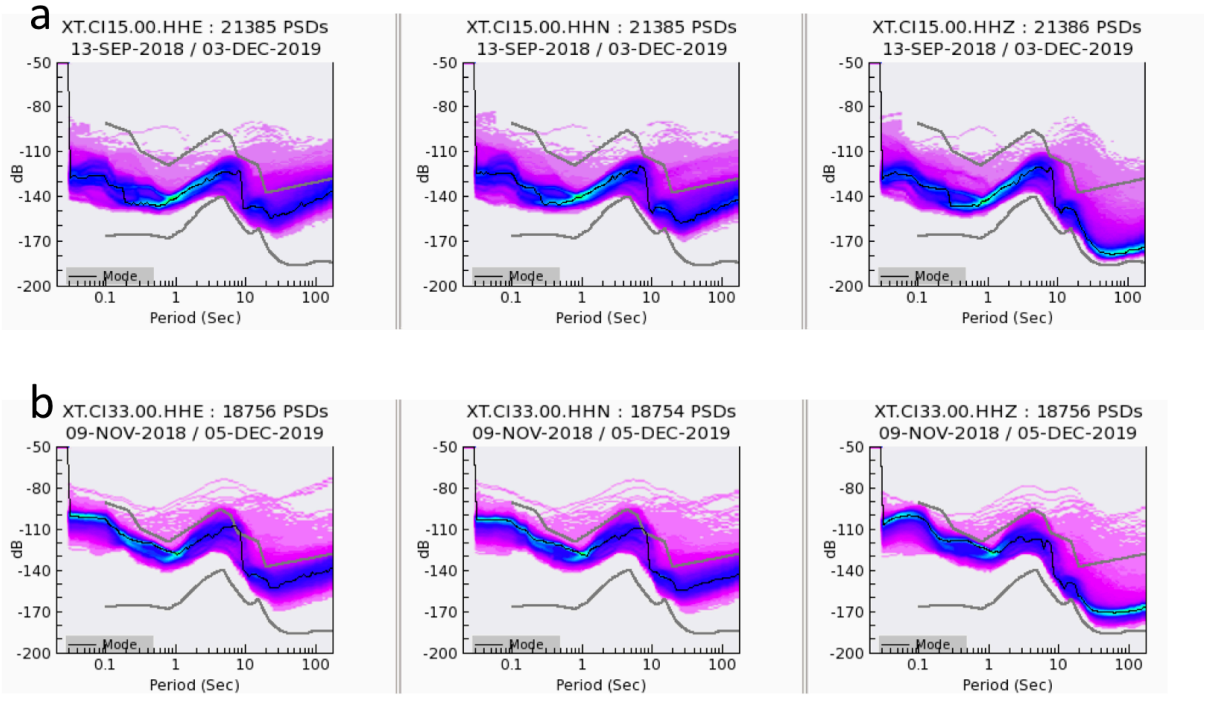

Figure S1: PDFs of PSDs at stations: (a) XT.CI15 and (b) XT.CI33 of the CIFALPS2 experiment computed for the whole operation period of each station. From left to right: east channel (HHE), north channel (HHN) and vertical channel (HHZ). The 2 grey curves in each plot are the standard low and high noise models (NLNM and NHNM; Peterson, 1993) defined

as extreme boundaries for permanent BB stations. The black curve is the mode of the probability density function (PDF).

S2- Receiver function analysis

Multichannel preprocessing (Rondenay, 2009):
For a given teleseismic event, the source time function $\overline{P}$ is estimated first by aligning and stacking the P components of P-S_V-S_H rotated seismograms of available station records. Then, the scattered wavefield P'-S_V-S_H is estimated for each station by subtracting the source time function $\overline{P}$ from the recorded P component (P'=P-$\overline{P}$). Finally, the estimated source wavefield is deconvolved from the estimated scattered wavefield P'-S_V-S_H in the frequency domain using a regularized least-square inversion with parameters adapted to each station record and each component.
A correct estimate of the source time function in the multichannel preprocessing requires a sufficient number of station records with high signal-to-noise ratio. We selected events in a longer time period for CIFALPS2 (2015-02 to 2020-07) than for CIFALPS (2012-06 to 2013-10) because the CIFALPS2 dataset was complemented by records of permanent stations (networks: CH, Swiss Seismological Service (SED) At ETH Zurich, 1983; FR, RESIF, 1995; GU, University of Genoa, 1967; IV, INGV Seismological Data Centre, 2006) and temporary stations from the AlpArray seismic network (network Z3; AlpArray Seismic Network, 2015; Hetényi et al., 2018). This provided additional receiver functions at the few permanent and AlpArray stations located along or close to the profile.

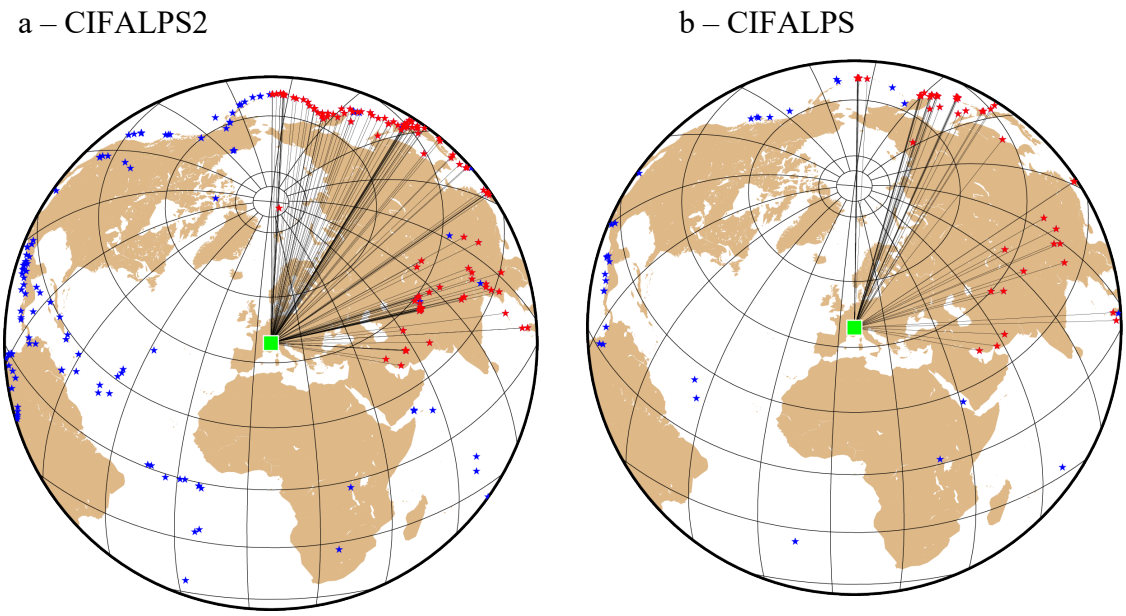

Figure S2: Maps of earthquake epicenters used in the receiver function studies. Red stars: selected events; blue stars: unselected events; green square: study region. a) CIFALPS2 experiment: 129 selected teleseismic events in the 0-100° back-azimuth range for the time period 2015-02 to 2020-07. b) CIFALPS experiment: 57 selected events in the 0-100° back-azimuth range for the time period 2012-06 to 2013-10.

S3- Jackknife tests of the CCP stacks

To test the robustness of the CCP stacks and estimate uncertainties, we used a jackknife resampling approach (Efron, 1982; Liu et al., 2016). For a CCP stack of N receiver functions, we created N/10 subsets with N/10 randomly selected RF deleted from the original dataset. A CCP stack was then computed for each of the subsets using the same procedure as for the original full dataset. The jackknife average of the N/10 resulting CCP stacks gave a new CCP section, whose uncertainty was estimated from the standard deviation of the N/10 subsets.
The jackknife testing procedure was applied to all profiles discussed in the main text. Results are shown in Fig. S3A for CIFALPS2, Fig. S3B for the ALP-N and ALP-S CIFALPS2 complementary short profiles, and Fig. S3C for CIFALPS. The jackknife averages are so close to the initial CCP stacks that the differences are almost undetectable. The jackknife standard deviation is generally smaller than 0.01 except beneath regions with thick sedimentary basins (Bresse graben and Po basin in Fig. S3A, Po basin in Fig. S3B-right and Fig. S3C), where thick poorly consolidated sediments result in lower-than-average signal-to-noise ratio and induce strong reverberations in the teleseismic records. A few individual stations of lower-than-average quality also increase the jackknife standard deviation of the bins they contribute to (for example: station located at distance ~20 km in Fig.S3B-left, station at distance ~230 km in Fig. S3C). To further document the robustness of our CCP stacks, we masked by a grey background the bins with averaged amplitude smaller than the standard deviation. The resulting CCP sections ("Jackknife average with threshold") still display the same features as the initial CCP stacks.
We conclude that these jackknife tests demonstrate the robustness of our CCP stacks.

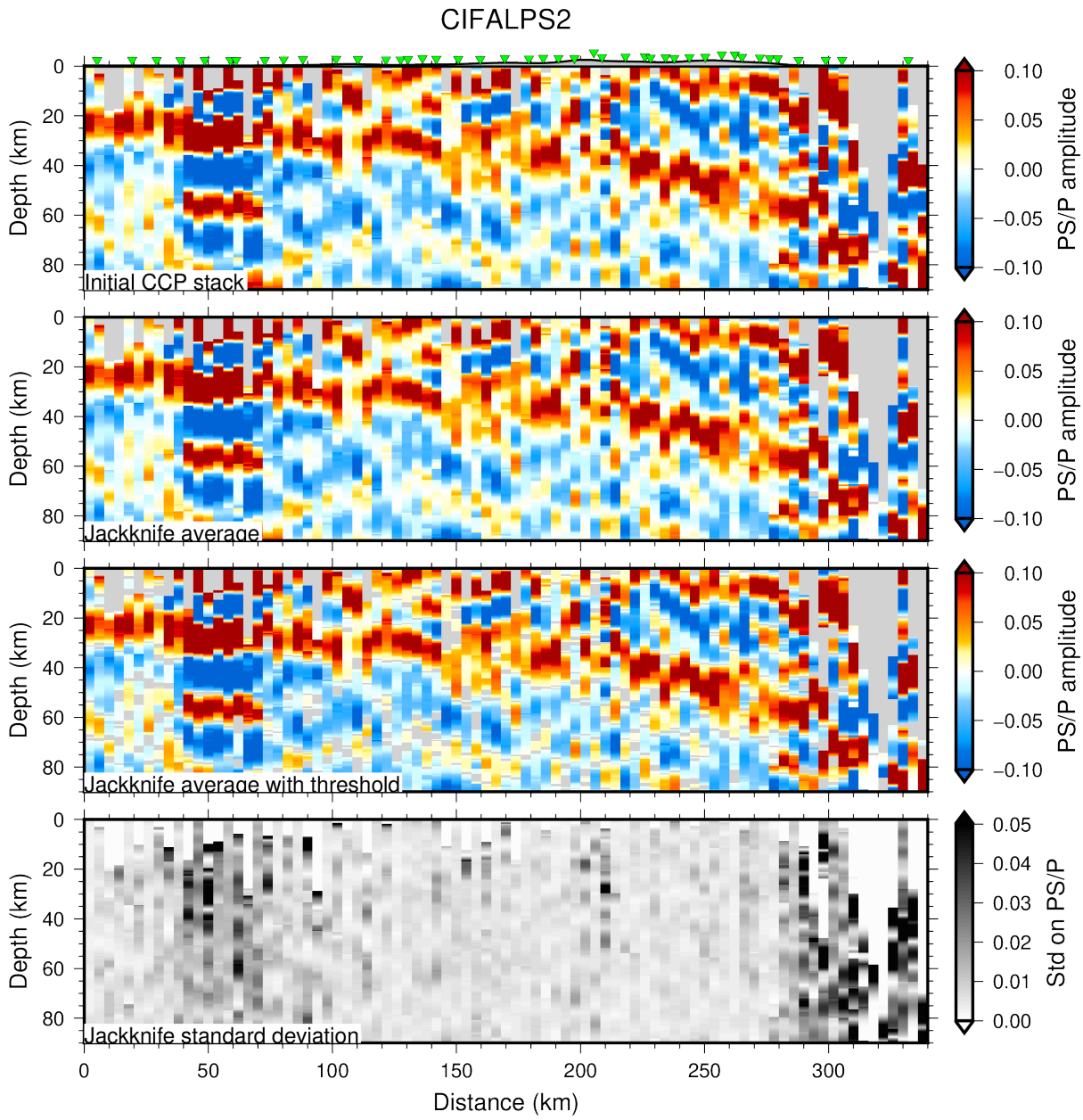

Figure S3A: Results of the jackknife test applied to the CCP (common conversion point) stack of the CIFALPS2 section (shown in Fig. 2d). From top to bottom: Standard CCP stack computed by stacking 1196 receiver functions (same as Fig. 2d); Jackknife average of the 119 CCP stacks computed by stacking subsets of 1077 randomly selected RF; Jackknife average where we only color plot the bins with averaged PS-to-P amplitude above the computed jackknife standard deviation; Jackknife standard deviation. Bins with higher-than-average standard deviation (dark grey to black color) are concentrated beneath the Bresse graben (distance 40-70 km) and the Po basin (distance>285 km), where thick poorly consolidated sediments result in lower-than-average signal-to-noise ratio and induce strong reverberations in the teleseismic records.

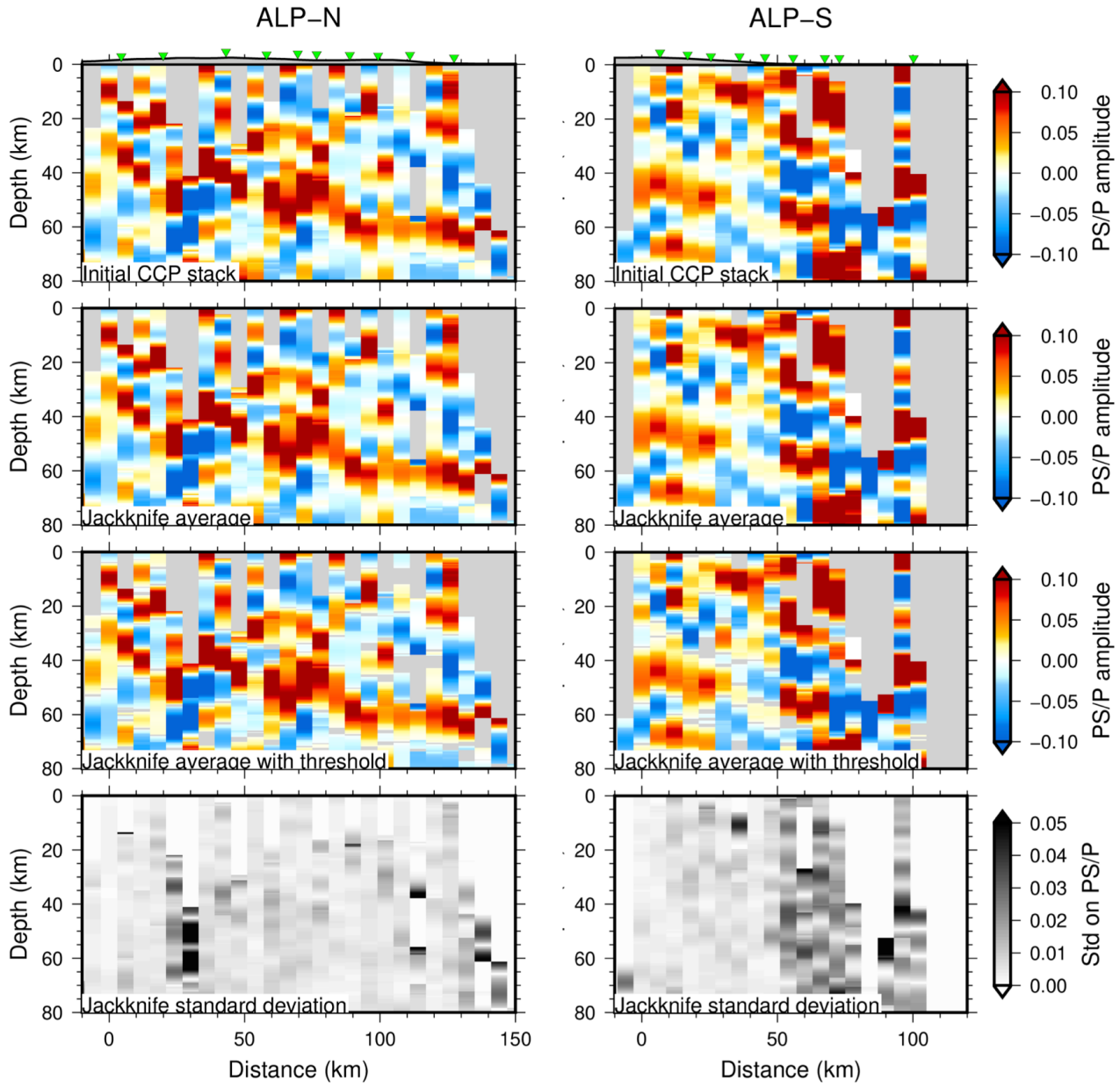

Figure S3B: Results of the jackknife test applied to the CCP stacks of the two ALP-N (left) and ALP-S (right) complementary profiles of the CIFALPS2 experiment (shown in Fig. 3c and 3g). The ALP-N CCP section is computed by stacking 328 RF, so the jackknife test is performed on 32 subsets of 296 RF each. The ALP-S section is computed by stacking 202 RF, with a jackknife test performed on 20 subsets of 182 RF. Same legend as Fig. S3A.

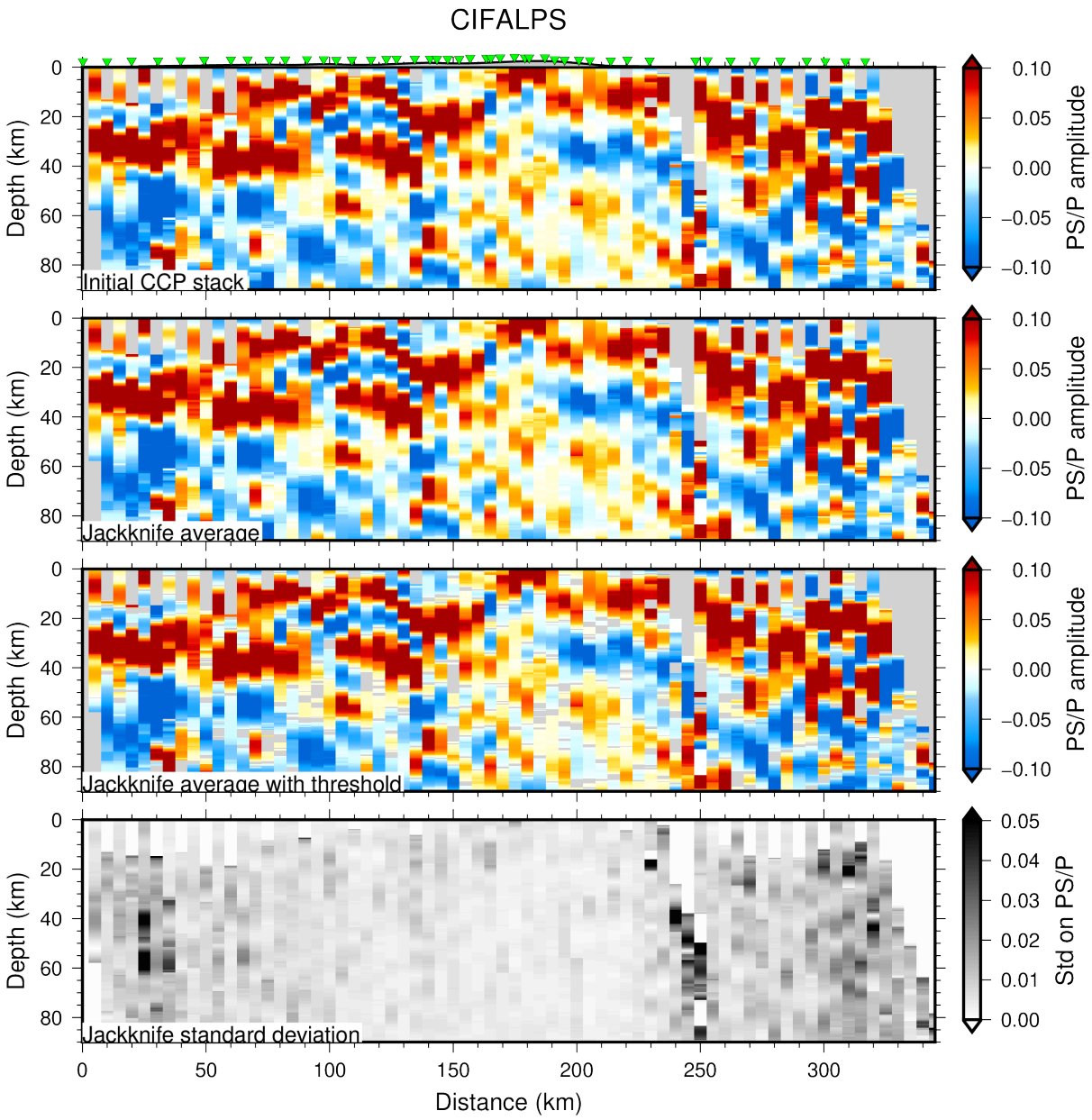

Figure S3C: Results of the jackknife test applied to the CCP stack of the CIFALPS profile (shown in Fig. 4d). The CIFALPS section is computed by stacking 1908 RF, with a jackknife test performed on 190 subsets of 1718 RF. Same legend as Fig. S3A.

S4- Comparison with the ECORS-CROP controlled-source seismic reflection section

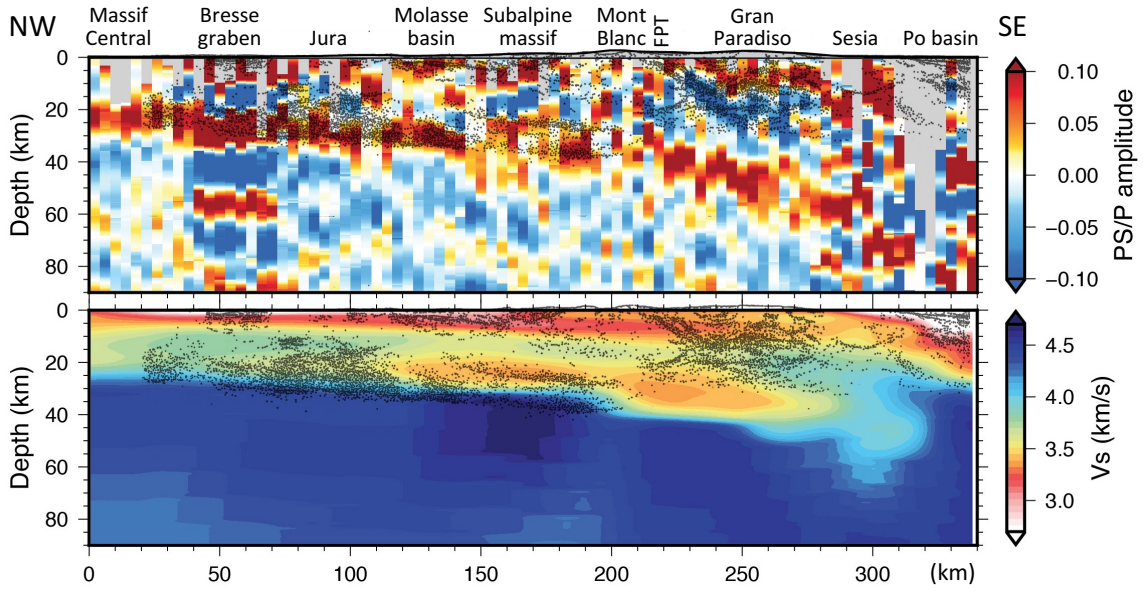

Figure S4: Depth-migrated line drawing of the ECORS-CROP CSS reflection profile overlaid on the Cifalps2 CCP stack (top) and the Vs section from Nouibat et al. (2022) (bottom). ECORS-CROP line drawing from Sénéchal & Thouvenot (1991). FPT: Frontal Penninic fault.

Supplemental reference list

Efron, B., 1982. The jackknife, the bootstrap, and other resampling plans, SIAM Press, Philadelphia.

Hetényi, G., et al., 2018. The AlpArray Seismic Network – a large-scale European experiment to image the Alpine orogeny, Surveys in Geophysics, 39, 1009–1033, doi:10.1007/s10712-018-9472-4

Liu, Z., J. Park, and S. Karato, 2016. Seismological detection of low-velocity anomalies surrounding the mantle transition zone in Japan subduction zone, Geophysical Research Letters, 43, 2480-2487, doi: 10.1002/2015GL067097.

McNamara D. E., & R. P. Buland, 2004. Ambient Noise Levels in the Continental United States, Bulletin of the Seismological Society of America 94 (4): 1517–1527, doi:10.1785/012003001

McNamara, D. E. & R. Boaz, 2011. PQLX: A seismic data quality control system description, applications, and users manual, USGS Open File report 2010-1292, doi:10.3133/ofr20101292

Peterson, J. R., 1993. Observations and modeling of seismic background noise, USGS Open-File Report 93-322, doi:10.3133/ofr93322

Péquegnat, C., et al., 2021. Résif-SI: a distributed information system for French seismological data, *Seismol. Res. Lett.*, 92(3), 1832-1853, doi:10.1785/0220200392.